Elucidating the biochemical parameters of scFvs influencing tonic CAR signaling

Master Thesis

For the attainment of the academic degree
“Diplom-Ingenieurin” (Dipl.-Ing.)

Mara Mitstorfer, BSc.

Supervisor

Univ. Prof. Dr. Christian Obinger
BOKU - University of Natural Resources and Life Sciences
Department of Chemistry

Co-supervisor

Dipl.-Ing. Dr. Michael Traxlmayr
BOKU - University of Natural Resources and Life Sciences
Christian Doppler Laboratory for Next Generation CAR T cells

Abstract

Chimeric antigen receptor (CAR) T cell therapy has shown unparallel successes in the treatment of hematologic malignancies. However, so far only CAR T cell therapies targeting the blood cell antigen CD19 have received FDA approval. CARs targeting other antigens failed to achieve similarly high response rates. One of the main obstacles associated with the failure of CAR T cell therapy is the development of T cell exhaustion as a result of ligand-independent tonic CAR signaling. This phenomenon has been associated with poor CAR T cell proliferation as well as poor persistence *in vivo* and has been observed for multiple CARs. Single chain variable fragments (scFvs) commonly used as CAR binding domains have been shown to play a pivotal role in causing tonic signaling. The lack of a systematic investigation of the scFv properties leading to tonic signaling in the CAR field prompted us to investigate whether readily measurable biochemical characteristics of scFvs can be correlated with the tonic signaling behavior of respective CARs. The overall objective was to find a predictive assay for scFv-related tonic signaling of CARs.
For that purpose, we selected a set of 16 different scFvs including subsets of favorable (little/no exhibition of self- and cross-interactions) and unfavorable (exhibition of self- and/or cross-interactions) biochemical characteristics with different thermal stabilities as well as one subset consisting of scFvs currently used in CARs. We fused the scFvs to identical CAR backbones and used flow cytometry to analyze their tonic signaling behavior using a reporter cell line. Importantly, the applied CAR and scFv designs were identical for all constructs to ensure comparability of the tonic signaling results.
We observed a strong trend for higher tonic signaling in CARs based on scFvs with unfavorable biochemical characteristics. This trend was independent of CAR expression levels. We then solubly expressed scFv candidates which were associated with interesting tonic signaling behavior in a quest to further analyze the observed trend with size exclusion chromatography (SEC)-multiangle light scattering (MALS) measurements. SEC-MALS measurements revealed the scFvs' propensity for aggregation and nonspecific binding to the column matrix. The soluble scFv expressions generally yielded low amounts of protein indicating low scFv stability. We could not identify a correlation between scFv aggregation and tonic signaling of respective CARs. However, we observed a potential link between late SEC elution and tonic CAR signaling, indicating a predictive value of the stickiness of scFvs for the tonic signaling behavior of respective CARs.
In summary, we show that scFv stickiness might play an important role in the induction of tonic CAR signaling. More precisely, the investigation of the nonspecific binding behavior of scFvs by SEC-MALS may provide valuable insight whether a scFv will induce tonic signaling when used as a CAR binding domain. In contrast, our data indicate that the aggregation behavior of solubly expressed scFvs does not constitute a suitable predictive assay for tonic CAR signaling.

Kurzfassung

Chimäre Antigen Rezeptor (CAR) T-Zelltherapie hat bemerkenswerte Erfolge in der Behandlung von malignen hämatologischen Erkrankungen erzielt. Jedoch, wurden bisher nur CAR T-Zelltherapien von der FDA zugelassen, die das B-Zell Antigen CD19 anvisieren. CARs, die gegen andere Antigene gerichtet sind, konnten bisher nicht an diese Erfolge anknüpfen. Eines der größten Hindernisse für CAR T-Zelltherapien ist die Entstehung von T-Zell Erschöpfung aufgrund von ligandenunabhängiger chronischer T-Zellaktivierung (‚tonic signaling'). Dieses Phänomen wurde mit geringer CAR T-Zellvermehrung sowie kurzer Persistenz der Zellen *in vivo* in Verbindung gesetzt und wurde mit diversen CARs beobachtet. Es wurde gezeigt, dass die als Bindungsdomäne häufig verwendeten scFvs (single chain variable fragments) eine entscheidende Rolle in der Entstehung von ‚tonic signaling' spielen. Der Mangel an einer systematischen Erforschung der dafür verantwortlichen scFv Eigenschaften im CAR Feld, veranlasste uns zu untersuchen, ob einfach messbare biochemische Eigenschaften von scFvs mit dem ‚tonic signaling' Verhalten von den jeweiligen CARs korreliert werden können. Das höhere Ziel war es, einen prognostischen Assay für scFv-bedingtes ‚tonic CAR signaling' zu finden.
Dafür wurde ein Set von 16 verschiedenen scFvs ausgewählt, welches aus Untergruppen von scFvs mit günstigen (wenig bis keine Selbst- und Kreuzinteraktionen) und ungünstigen (Selbst- und Kreuzinteraktionen) biochemischen Eigenschaften mit jeweils unterschiedichen thermischen Stabilitäten bestand. Zusätzlich wurde eine Untergruppe bestehend aus scFvs, welche derzeit in CARs Verwendung finden, gewählt. Alle scFvs wurden mit einem identischen CAR Grundgerüst fusioniert. Die CARs wurden in eine Reporter Zelllinie eingebracht und das ‚tonic signaling' Verhalten der CARs wurde mittels Durchflusszytometrie analysiert. Die CAR und scFv Designs waren identisch für alle Konstrukte um die Vergleichbarkeit der ‚tonic signaling' Resultate zu gewährleisten.
Wir beobachteten einen eindeutigen Trend für höheres ‚tonic signaling' in CARs basierend auf scFvs mit ungünstigen biochemischen Eigenschaften. Dieser Trend war unabhängig von der CAR Expressionsstärke. Nachfolgend wurden scFvs mit interessantem ‚tonic signaling' Verhalten löslich exprimiert um den beobachteten Trend mittels Größenausschlusschromatographie mit Multi-Winkel-Lichtstreuung (SEC-MALS) weiter zu analysieren. SEC-MALS Messungen zeigten das Aggregationsverhalten der scFvs auf, sowie die Neigung zu unspezifischer Bindung an die Säulenmatrix. Die Protein-Ausbeuten bei der löslichen Expression waren generell sehr gering, was womöglich auf eine geringe scFv Stabilität zurückzuführen ist. Wir konnten keine Korrelation zwischen scFv Aggregation und dem ‚tonic signaling' Verhalten der jeweiligen CARs feststellen. Jedoch beobachteten wir eine potenzielle Verbindung zwischen später SEC Elution und ‚tonic CAR signaling'. Dies impliziert einen Vorhersagewert des unspezifischen Bindungsverhaltens von scFvs für das ‚tonic signaling' Verhalten von entsprechenden CARs.
Zusammenfassend zeigen wir, dass unspezifisch-bindende scFvs womöglich eine wichtige Rolle in der Verursachung von ‚tonic CAR signaling' spielen. Die Analyse des unspezifischen Bindungsverhaltens von scFvs könnte einen wertvollen Hinweis darstellen, ob ein scFv bei Verwendung als CAR Bindungsdomäne zu ‚tonic signaling' führen wird. Im Gegensatz dazu, scheint die Analyse des Aggregationsverhaltens von löslich exprimierten scFvs kein angemessener prognostischer Assay für ‚tonic signaling' zu sein.

Acknowledgements

First of all, I want to thank Christian Obinger for providing me the opportunity to do my Master thesis in the Protein Biochemistry group.
Second, I want to thank Michael Traxlmayr for inspiring me to absolve my Master thesis in the field of cancer immunotherapy in the course of his lectures and for giving me the possibility to do so within this interesting project.
Most importantly, I am grateful for the exceptional supervision by Charlotte Zajc. Thank you for providing advice and assistance all along, for diligently answering any arising questions, for sharing your expertise in the lab and last but not least for always being so attentive, kind and supportive.

On top of that, I would like to thank the whole team of the CD laboratory for Next Generation CAR T cells for the many discussions and your invaluable input. My special thanks go to Michael Traxlmayr, Manfred Lehner, Charlotte Zajc and Benjamin Salzer. I greatly enjoyed your genuine and inspiring enthusiasm for CAR research.
In addition, I want to thank Benjamin Salzer for kindly providing his Nur77 Jurkat reporter cell line and Patrick Gano for culturing the cells at the CCRI.

Of course, I also want to thank the whole BioB for creating such a fun and caring working atmosphere. I greatly enjoyed working in such a pleasant environment.
Finally, I want to thank my parents for always supporting me, and my sister and friends for patiently listening to my countless trains of thought and for their remarkable effort to try to make sense of them.

Acronyms

ALL acute lymphoblastic leukemia

APC antigen presenting cell

BSA bovine serum albumin

CAR chimeric antigen receptor

CDR complementarity-determining region

CRS cytokine release syndrome

dNTP's desoxyribonucleotide triphosphates

DPBS Dulbecco's phosphate buffered saline

DSC differential scanning calorimetry

FACS fluorescence activated cell sorting

FBS fetal bovine serum

FR framework region

HPLC high-performance liquid chromatography

HSA human serum albumin

IMAC immobilized metal affinity chromatography

LB lysogeny broth

mAb monoclonal antibody

MALS multiangle light scattering

MES 1,3,5-trimethylbenzene

MFI mean fluorescence intensity

MHC major histocompatibility complex

mKO2 mKusabiraOrange2

Mw molecular weight

PBS phosphate buffered saline

PCR polymerase chain reaction

PEI polyethylenimine solution

scFv single chain variable fragment

SD standard deviation

SEC size-exclusion chromatography

TAA tumor associated antigen

TAE tris-acetate-edta

TCR T cell receptor

TGS tris/glycine/SDS

TN1 tryptone N1

$\mathbf{V_H}$ variable domain of the heavy chain

$\mathbf{V_L}$ variable domain of the light chain

Contents

List of Figures

List of Tables

Chapter 1

Introduction

The advent of cancer immunotherapy has revolutionized the field of cancer therapy. Among the diverse repertoire of cancer immunotherapies one of the most promising approaches is called chimeric antigen receptor (CAR) T cell therapy. Although T cells have the natural ability to fight cancer to some extent, tumors commonly develop mechanisms to escape immunosurveillance [1]. Moreover, immune recognition of cancer cells is often troublesome as cancer cells are inherently 'self' as opposed to pathogens. Therefore, harnessing T cells to recognize tumor associated antigens (TAAs) is a useful tool in the fight against cancer. CARs are synthetic receptors used to redirect the patient's T cells towards TAAs. For CAR T cell therapy, patient-derived T cells are genetically engineered to express CAR molecules on the T cell surface, resulting in autologous immune cells targeting tumor cells in the patient's body. Owing to single chain variable fragments (scFvs) or other antigen-binding moieties used in CARs, TAAs can be targeted in a major histocompatibility complex (MHC)-independent fashion. This is advantageous, as downregulation of MHC class I molecules constitutes a major immune escape mechanism of cancer cells [2], [3]. In 1993, the group of Zelig Eshhar proposed the first scFv-based CAR prototype [4]. Since then, CARs have undergone a long journey of development, eventually leading to promising clinical trials for CAR T cell therapies targeting the B cell antigen CD19 and culminating in the FDA approval of the first CAR T cell therapies in 2017 [5]–[8].

1.1 CAR T cells in the clinics

Novartis was the first company that received FDA approval for a CAR T cell product back in 2017. Kymriah™ (tisagenlecleucel) has been approved for the treatment of pediatric and young adult patients with B cell acute lymphoblastic leukemia (ALL). Only a few months later Yescarta™ (axicabtagene ciloleucel) from Kite pharma (now a Gilead Company) received approval for the treatment of adults suffering from relapsed or refractory large B cell lymphoma [9]. Both CAR T cell products target the antigen CD19 which is expressed on B cells. With both CAR T cell therapies impressive complete remission rates of up to 83% for Kymriah™ (ELIANA trial) and 58% for Yescarta™ (ZUMA trial) were achieved in patients who had undergone heavy pre-treatment [10]. Despite these successes, the field of CAR T cell therapy also faces major challenges such as severe side effects and the translation of CAR T cell therapies to solid tumor types. Therefore, much effort is undertaken to develop safer therapies and to expand the therapy's success beyond B cell malignancies [11] (section 1.5).

1.2 Production of CAR T cells

The production of CAR T cells starts with the collection of T cells from the patient in a process called apheresis. The obtained cells are activated *ex vivo* with antibody-coated beads imitating

the stimulation with antigen presenting cells (APCs). The activated T cells are then transduced with a plasmid encoding the CAR molecule, most commonly by means of a lentivirus or a retrovirus. After a period of expansion, the modified cells are reinjected into the lymphodepleted patient. The prior lymphodepletion most commonly achieved with chemotherapy allows for better CAR T cell expansion and engraftment [12]. The production process is illustrated in Figure 1.1.

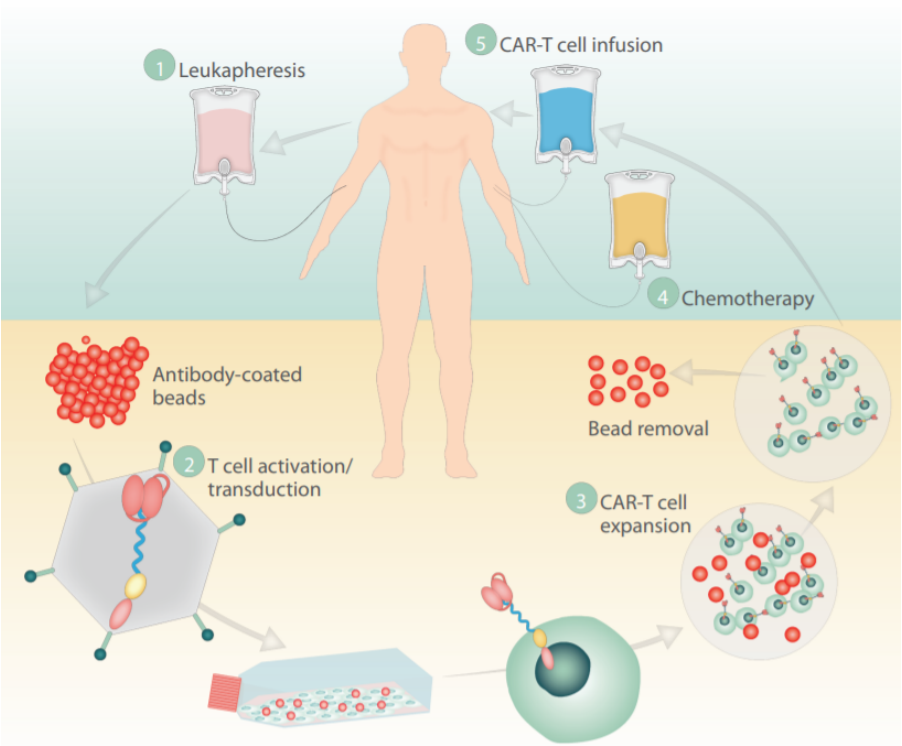

Figure 1.1: Shematic representation of the CAR T cell production process. Figure by [13]

1.3 CAR design

CARs are designed in a modular fashion and consist of an extracellular binding domain (most commonly a scFv), an optional spacer domain, a transmembrane domain and intracellular signaling domains. The first CAR designs, also referred to as first-generation CARs, relied merely on the T cell receptor (TCR)-derived CD3ζ-endodomain which delivers the T cell activation signal. Due to lack of co-stimulatory domains these CARs did not provide the secondary signal required for full T cell activation. As a result, the T cells exhibited weak expansion potentials and poor persistence *in vivo* [9], [14]. This problem could be tackled with the development of second- and third-generation CARs incorporating one or more co-stimulatory domains, respectively. Such improved CARs have been linked with higher persistence and a better clinical response [15], [16]. The different generations of CARs are depicted in Figure 1.2. The most commonly used and best studied co-stimulatory domains are CD28 and 4-1BB. Other options are OX-40, ICOS, CD27 or MyD88/CD40 [14].

1.4 ScFvs and scFv aggregation

ScFvs are engineered antibody fragments that consist of the variable domain of the light chain (V_L) and the variable domain of the heavy chain (V_H) derived from a full-length monoclonal antibody (mAb). The domains are connected with a flexible peptide linker. Thus, scFvs comprise

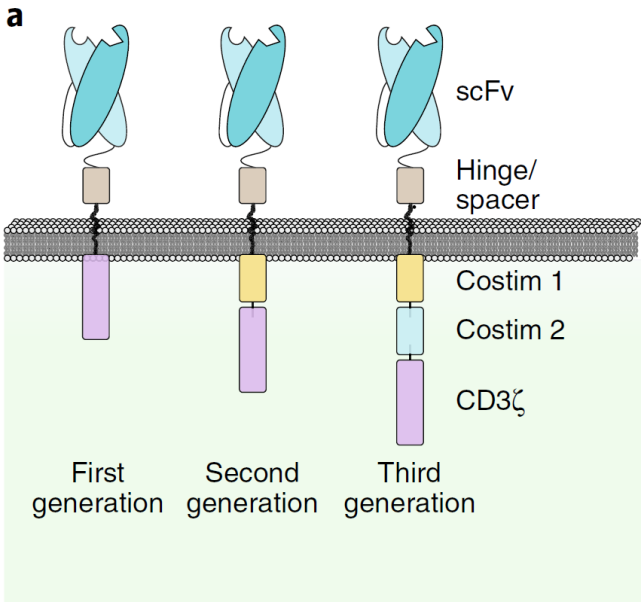

Figure 1.2: Different generations of CARs. Figure by [14]

the full antigen-binding site in one single polypeptide. Usually, the achieved antigen affinities are similar to those achieved with the parental mAbs [17]. Each variable domain contains three complementarity-determining regions (CDRs) and four framework regions (FRs). While CDRs form loops and make up the unique antigen-binding site, FRs comprise beta-strands and additional loop regions and have crucial function in scFv stability and integrity [18]. In terms of domain orientation, the V_H-V_L orientation is often favored because it leaves a bigger distance between the protein linker and the third CDR of the heavy chain which usually is crucial for antigen-binding. Nevertheless, in some cases V_L-V_H orientation has been associated with increased expression and antigen-binding [19]. In other cases, similar surface expression and antigen-binding have been reported for either orientation [20]. Therefore, there is no general conclusion about preferred orientations of the V_L and V_H domains in scFvs.

Under certain conditions, scFvs have the tendency to aggregate or to form multimers [18], [21]. Examples for such multimers are diabodies and triabodies as depicted in Figure 1.3.

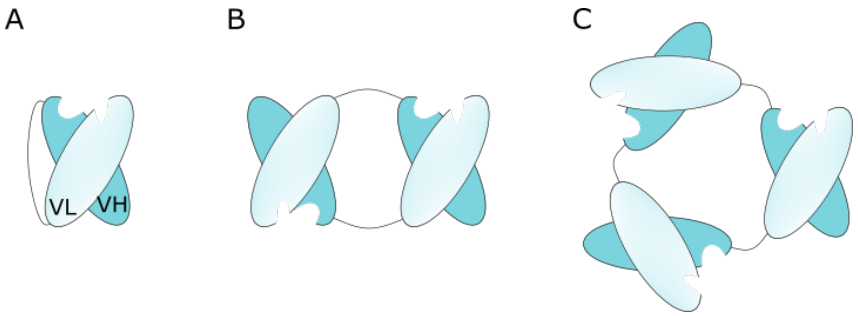

Figure 1.3: Illustration of a single scFv (A), a diabody (B) and a triabody (C)

A major determining factor for scFv aggregation is the stability of the V_H:V_L interface which is primarily defined by hydrophobic interactions between surface exposed residues of the framework building beta sheet regions [22]. Suboptimal interface stability can lead to transient separation of the domains resulting in the exposure of hydrophobic patches. This exposure may favor scFv aggregation or allow for 'protein domain swapping' where complementary domains of adjacent scFvs interact with each other to form diabodies. The resulting scFv-diabody equilibrium is shown in Figure 1.4. In addition to the V_H:V_L interface stability, the scFv stability is also

determined by the intrinsic domain stabilities of the V_H and V_L domains which, in turn, is greatly influenced by intradomain disulfide bonds between cysteine residues [22].

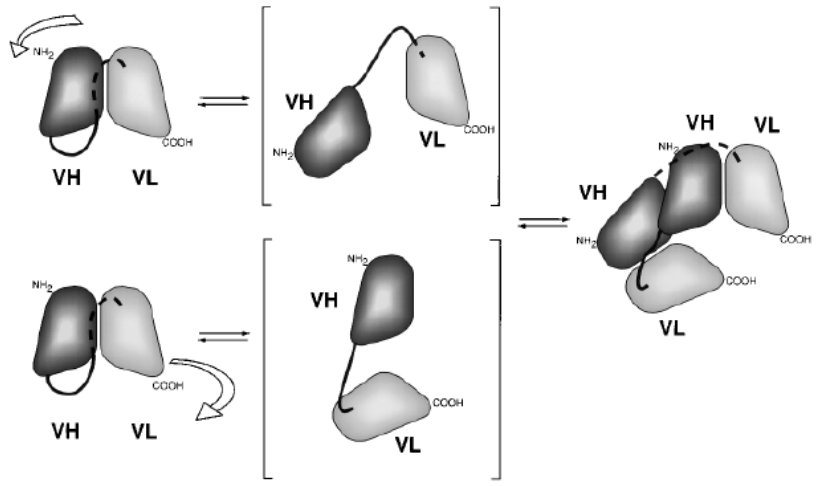

Figure 1.4: ScFv-diabody equilibrium. Figure by [22]

The linker length also greatly influences oligomerization behavior. Short linkers of up to 15 amino acid residues strongly favor the formation of oligomers. In contrast, long linkers with 15-25 amino acid residues favor the monomeric state as they provide the necessary length required to reach from one C-terminus to the N-terminus of the second domain, which is a prerequisite for correct domain pairing [22]. The most commonly used linker type is the (G4S)n linker, consisting of repeats of four glycine residues and one serine residue [23]. Alternative linkers have also been developed such as the 'Whitlow linker' exhibiting a length of 18 aa residues. This linker contains a proline residue as well as charged residues to achieve high proteolytic stability [24].

1.5 Challenges in CAR T cell therapy

Despite the impressive clinical responses achieved with the anti-CD19 CAR T cell therapies, major challenges remain to be solved in the CAR field.

1.5.1 Adverse events

To begin with, CAR T cell therapy is commonly associated with severe side-effects such as cytokine release syndrome (CRS) and neurological toxicities [25]–[27]. CRS, the most common toxicity of CAR T cell therapies, is the result of extensive cytokine and chemokine release by activated CAR T cells and other immune cells. The disease can have mild to severe courses. Typical constitutional symptoms include fever, malaise, anorexia, and myalgias [26]. Organ-specific symptoms may comprise tachycardia/hypotension, capillary leak, cardiac dysfunction, renal impairment, hepatic failure and others [25]. In severe cases, CRS can lead to life-threatening multiorgan dysfunction [26], [27].

Neurological toxicity represents the second most-common toxicity of CAR T cell therapies [26]. Symptoms are wide-ranging including confusion, delirium, expressive aphasia, obtundation, myoclonus, and seizure [25]. The severity of symptoms can change rapidly. Therefore, intensive patient monitoring is from utmost importance. Although symptoms are reversible in most cases, fatal courses have also been reported [26]. The causing mechanisms of these neurotoxicities have not yet been entirely resolved. However, there is evidence that cytokines lead to endothelial activation and increased permeability of the blood-brain barrier allowing cytokines and CAR T cells to enter the cerebrospinal fluid [28].

1.5.2 Treatment of nonhematological malignancies

The expansion of the application of CAR T cell therapies to solid tumors has turned out to be cumbersome. Thus far, most clinical trials of CAR T cell therapies for solid tumors yielded poor results [29]. One major problem is the scarcity of tumor-specific antigens in solid tumors. Shared antigen expression by normal cells can lead to severe on-target/off-tumor toxicities [25], [30]. In contrast, the antigen CD19 is exclusively expressed on B cells which limits off-target effects to B cell aplasia. B cell aplasia can be compensated with immunoglobulin-replacement therapy [8]. Other obstacles to be solved include tackling tumor antigen loss, trafficking the T cells to the tumor site, and dealing with the immunosuppressive tumor microenvironment [31], [32]. These challenges are drivers for the development of innovative CAR designs and for the exploration of diverse candidate targets for different tumor types.

1.6 CAR efficacy – tonic signaling and CAR T cell exhaustion

T cell exhaustion constitutes a major limiting factor for CAR T cell efficacy [33]. The development of an exhausted phenotype can not only arise from chronic antigen stimulation but also from antigen-independent tonic CAR signaling as demonstrated by Long et al. [34]. T cell exhaustion is commonly defined by upregulation of exhaustion-mediated transcription factors and a distinct transcriptional profile including increased expression of inhibitory receptors such as PD-1, TIM-3 and LAG-3. This condition is associated with poor *in vivo* persistence and efficacy as well as reduced cytokine production [34], [35].

1.6.1 Influence of the scFv used as CAR binding domain

The tendency of scFvs to form aggregates as described in section 1.4 may not only relate to isolated entities but also to scFvs which are incorporated in CARs. Such scFv aggregation may result in CAR clustering on the T cell surface. In a study performed by Long and colleagues it was concluded that CAR clustering causes ligand-independent tonic signaling of CARs which shall be further referred to as tonic signaling [34]. The group discovered tonic signaling in CAR T cells equipped with a scFv targeting the disialoganglioside GD2 on sarcoma (14g2a scFv). Further, they could link the tonic signaling behavior with the development of an exhausted phenotype and poor *in vivo* performance of the anti-GD2 CAR. In contrast, no such behavior was found upon investigation of the clinically successful anti-CD19 CAR based on the FMC63 scFv. CAR clustering is illustrated in Figure 1.5 which shows T cells expressing the FMC63-based anti-CD19 CAR on the left and the 14g2a-based anti-GD2 CAR on the right. Both CARs contained the CD28 co-stimulatory domain. The CAR molecules have been fused to a fluorescent protein to allow for CAR imaging. Comparing the two images, the anti-CD19 CAR seems to be more evenly distributed on the T cell surface. Long and colleagues interpreted the uneven surface distribution of the GD2 CAR as CAR clustering [34].

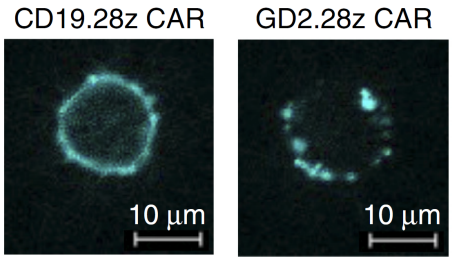

Figure 1.5: Fluorescence microscopy image of CAR T cells expressing CAR-Cerulean fusion proteins (blue) - left: FMC63-based anti-CD19 CAR, right: 14g2a-based anti-GD2 CAR. Figure by [34]

Importantly, the exhaustive phenotype is not unique to T cells carrying the anti-GD2 CAR with the 14g2a scFv but also occurs in other CAR T cells. Aside from the anti-GD2 CAR and the anti-CD19 CAR, Long and colleagues investigated three other CARs, all of which displayed tonic signaling to different degrees. Two of these CARs were specific for the CD22 antigen based on the HA22 scFv and the m971 scFv, respectively, and one was directed against the ErbB2 antigen (based on the 4D5 scFv) [34].

To gain insight into the aggregation-causing elements of the scFvs, the group produced hybrid CARs with exchanged FRs. Replacement of the FRs of the FMC63 scFv (anti-CD19) with FRs from the 14g2a scFv (anti-GD2), triggered the development of an exhausted phenotype in the anti-CD19 CAR. This observation implies that the tonic signaling behavior is strongly associated with the scFv's FRs, potentially linking the overall stability of scFvs to their capability to oligomerize and subsequently, lead to tonic signaling. However, vice versa, with the anti-GD2 CAR carrying the FMC63 FR, tonic signaling could not be analyzed as this CAR version showed no expression [34]. Consequently, one potential strategy to address tonic signaling could be stability engineering of scFvs as explained by Ajina and Maher [36]. Figure 1.6 illustrates possible starting points for stability engineering. Among others, these include the optimization of the scFv's net charge, the engineering of disulfide bonds between the V_H and V_L domains or stability engineering of the V_H:V_L interface e.g. by introducting amino acids capable of hydrogen bond formation [36].

As a side note, Fujiwara et al. showed that the FR sequence also has great impact on the CAR expression efficiency and that CDR-grafting to stable FRs can enhance the expression levels of CARs [20].

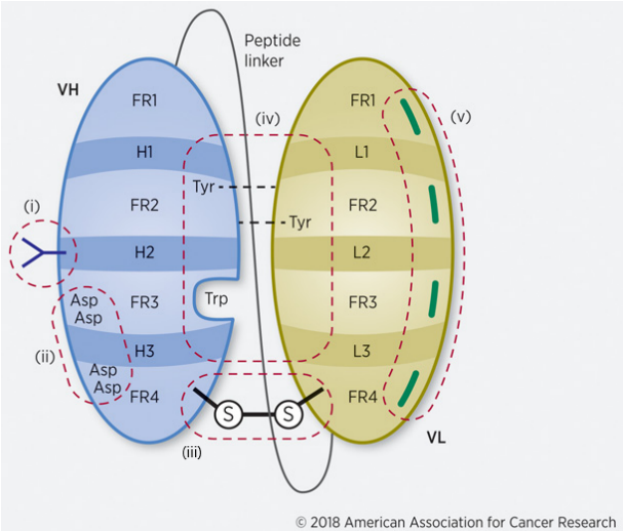

Figure 1.6: Approaches for stability-engineering of scFvs. (i) Glycosylation to compensate for hydrophobic residues; (ii) change of the scFv's net charge; (iii) incorporation of disulfide bridges; (iv) & (v) optimization of the stability of the domain interface using computational modeling [36]. Figure adapted from [36]

1.6.2 Influence of the co-stimulatory domain

As already touched on above, CD28 and 4-1BB are the most commonly used co-stimulatory domains in CARs. Although clinical trials report similar response rates of CARs incorporating either of the two endodomains, noticeable differences were observed in terms of effector functions, expansion and persistence. While CD28-co-stimulation promotes differentiation into a potent but short-lived effector phenotype with primarily glycolytic metabolism, 4-1BB co-stimulation confers enhanced T cell expansion and favors the generation of central memory T cells with primarily oxidative metabolism (Figure 1.7) [37]–[39]. Additionally, increased persistence of CAR 4-1BB T

cells in patients has been described in a multitude of publications [9], [12], [14]. The reason for these differences seems to lie mainly in a major divergence in the strength of the conferred signals rather than the activation of distinct signaling pathways [35]. According to a study by Salter et. al, CD28-co-stimulation is associated with faster and more extensive phosphorylation of signaling intermediates, resulting in the differentiation into an effector phenotype with a fast and strong anti-tumor response. The strong signaling could be correlated with the development of T cell dysfunction explaining the poor persistence of CD28-co-stimulated CAR T cells. In contrast, signaling through 4-1BB has been shown to be slower and lower in intensity. Despite this, *in vivo* efficacy was comparable with CD28-co-stimulated CAR T cells. No signs for exhaustion could be detected [35].

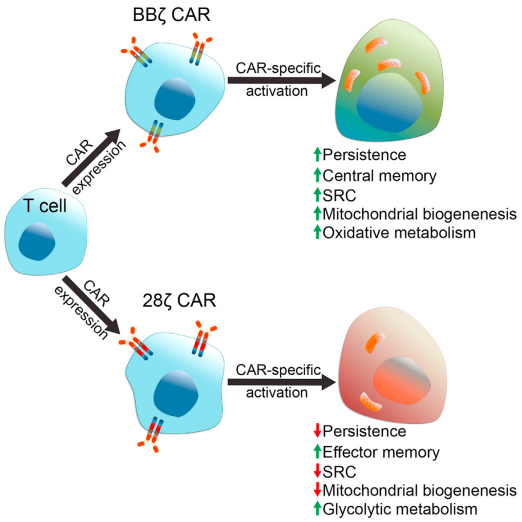

Figure 1.7: Differential effects of CD28-co-stimulation and 4-1BB-co-stimulation on the CAR T cell phenotype. Figure by [37]

Chapter 2

Aims

Chimeric antigen receptor (CAR) T cell therapy has achieved great success rates in patients suffering from B cell malignancies. Unfortunately, the treatment of other cancers has turned out to be more cumbersome. Adding to other challenges, the CAR T cell efficacy is commonly hampered by the development of CAR T cell exhaustion. T cell exhaustion as a result of tonic ligand-independent CAR signaling has been associated with the subsequent absence of *in vivo* proliferation and has been shown to occur to varying degrees in multiple CARs. Among other CAR elements, single chain variable fragments (scFvs) have been shown to have a crucial impact on tonic CAR signaling [34], [40]. As the development of new CAR T cell products is a highly laborious and costly process, it would be desirable to be able to predict whether a scFv candidate leads to tonic signaling when used as a CAR binding domain.

To our knowledge, no study has yet systematically investigated the role of scFvs in the development of tonic signaling of CARs. We therefore aimed to correlate biochemical characteristics of scFvs with the tonic signaling behavior of respective CARs by fusing a set of different scFvs to identical CAR backbones and analyzing their tonic signaling behavior using a reporter cell line. The CAR and scFv designs should be the same for all constructs to allow for comparability of the tonic signaling results as the CAR design has a great influence on the tonic signaling behavior.

The first objective was to gather a suitable scFv selection for the analysis. The selection should comprise scFvs with a wide range of different biochemical properties including sticky and/or aggregation-prone scFvs as well as scFvs which are not susceptible to self- and cross-interactions. We hypothesized that sticky and/or aggregation-prone scFvs lead to higher tonic signaling when used as a CAR binding domain than scFvs which are neither sticky nor aggregation-prone. Additionally, the selection should include scFvs which are currently used in CARs and whose tonic signaling behavior has already been reported in previous studies.

Next, the CARs which incorporate the scFvs from our selection should be transiently expressed in Nur77 Jurkat reporter cells. The CAR expression levels as well as the extent of tonic signaling should be determined for each CAR using flow cytometry to investigate any correlation between the induction of tonic signaling and biochemical properties of the used scFv.

Further, we aimed to solubly express scFvs with interesting tonic signaling behavior in HEK cells in order to analyze their aggregation and nonspecific binding behavior by size exclusion chromatography (SEC)-multiangle light scattering (MALS). We hypothesized that scFvs which were associated with tonic signaling would exhibit higher aggregation and/or would elute later from the column due to nonspecific binding to the column material. The objective was to determine whether SEC-MALS measurements of scFvs constitute a suitable approach for predicting the scFvs' performance as CAR binding domains in regard to tonic signaling.

Chapter 3

Materials and Methods

3.1 Materials

3.1.1 Laboratory Equipment

Table 3.1: Laboratory equipment

Equipment	**Manufacturer**
Arktik Thermal Cycler	Thermo Scientific
Gel Dox XR+ Gel Documentation System	Bio-Rad
Constant Voltage Power Supply (Model 1000/500)	Bio-Rad
Thermomixer comfort	Eppendorf
Centrifuge 5424	Eppendorf
Centrifuge 5415D	Eppendorf
Heraeus Multifuge 3S-R	Heraeus
Heraeus Multifuge X1 Centrifuge Series	Thermo Scientific
Sorvall RC6 centrifuge	Thermo Scientific
DeNovix DS-11 FX	DeNovix
Microscope	Carl Zeiss
Labscale TFF diafiltration system	Millipore
HPLC Prominence LC20 System	Shimadzu
SPD-M20A UV/VIS Photodiode Array Detector	Shimadzu
RID-10A Differential Refracotmetric Detector	Shimadzu
MALS Dawn8+	Wyatt
Automated PEAQ-DSC	Malvern Analytical
Autoclave HiCLave HG-80	HCM Europe
Laminar flow hood NordicSafe Class II Safety cabinet	Esco Micro Pte Ltd
Incubator and shaker 3033	GFL
Incubator Heracell 240i	Heraeus
Scale XS204	Mettler Toledo
Scale Entris	Sartorius
Vortex mixer Genie 2	Scientific Industries Inc.
Pipetboy Pipetus	Hirschmann Laborgeräte
CASY cell counter	OMNI Life Science
Electroporator Gene Pulser Xcell	Bio-Rad Laboratories
Flow Cytometer BD LSRFortessa	BD Biosciences

3.1.2 Disposables

Table 3.2: Disposables

Disposables	**Manufacturer**
Serological pipettes (2, 5, 10, 25 and 50 mL)	Greiner Bio-One
CELLSTAR Polypropylene Tubes, conical (15, 50 mL)	Greiner Bio-One
Pipette tips (200 µL, 1000 µL)	Gilson
Dual filter tips (10, 20, 100, 200, 1000 µL)	Eppendorf
Cell culture Erlenmeyer flasks, vented	Thermo Scientific
Petri dishes	Thermo Scientific
Microtubes (1.5 mL, 2 mL)	Eppendorf
Cryo tubes (2 mL)	Thermo Scientific
Fluorescence activated cell sorting (FACS) tubes, 5 mL	Becton Dickinson
Well plates (6, 12, 24, 48 wells)	Thermo Scientific
Tissue culture flasks:	
T25, T75, T175 and T182.5	Thermo Scientific
CASYcups	OMNI Life Science
Electroporation cuvettes 4 mm	VWR
Amicon Ultra (0.5 and 15 mL) Centrifugal Filter (10 kDa MWCO)	Merck Group
0.1 µm Ultrafree MC VV centrifugal filter	Merck Group

3.1.3 Kit systems

Table 3.3: Kit systems

Kit	**Manufacturer**
Monarch PCR & DNA cleanup kit	New England Biolabs
Monarch DNA gel extraction kit	New England Biolabs
Monarch plasmid miniprep kit	New England Biolabs
NucleoBond Xtra Midi/Maxi kit	Macherey Nagel
mMESSAGE mMACHINE T7 ULTRA Transcription Kit	Thermo Scientific
RNeasy mini kit	Qiagen

3.1.4 Buffers, media and solutions

Table 3.4: Media, additives and solutions for mammalian cell cultivation and experiments

Media, additives and solutions	Manufacturer
RPMI 1640 with GlutaMax-I	Thermo Scientific
RPMI 1640 without phenolred	Thermo Scientific
Opti-MEM	Thermo Scientific
Fetal bovine serum (FBS)	Sigma-Aldrich
Penicillin/Streptomycin (P/S)	Gibco
FreeStyle™ F17 Expression Medium	Thermo Scientific
L-Glutamine (200 mM)	Gibco
Pluronic F-68 (10% solution)	Gibco
G418 (50 mg/mL)	Millipore
10x Dulbecco's phosphate buffered saline (DPBS)	Sigma-Aldrich

Table 3.5: Complete media and solutions for prokaryotic and mammalian cell culture

Complete media and solutions	Composition
Lysogeny broth (LB)	10 g/L peptone 5 g/L yeast extract 200 mM NaCl Kanamycin: 50 µg/mL
LB agar	10 g/L peptone 5 g/L yeast extract 200 mM NaCl 10 g/L agar Kanamycin: 50 µg/mL
HEK293 6E medium	FreeStyle F17 Expression Medium 4 mM L-Glutamine 0.1% Pluronic F-68 25 µg/mL G418
RPMI culture medium for Jurkat reporter cells	RPMI 1640 with GlutaMax-I 10% FBS 1% P/S
Polyethylenimine solution (PEI) solution (pH 6.9-7.1)	Milli-Q water 1 g/L PEI 25K pH adjustments with HCl and NaOH
Tryptone N1 (TN1) solution (20% w/v)	FreeStyle F17 Expression Medium 200 g/L TN1 4M L-Glutamine 0.1% pluronic F-68
Glucose solution (10% (w/v))	Milli-Q water 100 g/L glucose

Table 3.6: Diverse buffers

Buffers	Composition
TALON purification – Equilibration buffer (pH 8)	1.86 g/L sodium phosphate monobasic 9.25 g/L sodium phosphate dibasic heptahydrate 17.5 g/L NaCl pH adjustments with HCl and NaOH
TALON purification – Wash buffer 1	Equilibration buffer 5 mM imidazole
TALON purification – Wash buffer 2	Equilibration buffer 15 mM imidazole
TALON purification – Elution buffer	Equilibration buffer 250 mM imidazole
TALON purification – Regeneration buffer	3.94 g/L 1,3,5-trimethylbenzene (MES) 17.4 g/L NaCl
FACS buffer	1xphosphate buffered saline (PBS) 1% human serum albumin (HSA) 0.02% sodium azide
SEC running buffer	1xPBS 200 mM NaCl

3.1.5 Enzymes and antibodies

Table 3.7: Enzymes and antibodies

Enzymes and antibodies	Provider
NotI-HF restriction enzyme	New England Biolabs
BamHI-HF restriction enzyme	New England Biolabs
Q5 Hot Start High-Fidelity DNA Polymerase	New England Biolabs
NEBuilder HiFi DNA Assembly Master Mix	New England Biolabs
DpnI restriction enzyme	New England Biolabs
APC anti-DYKDDDDK (clone L5, Isotype RatIgG2a, lambda)	BioLegend

3.1.6 Cell lines and strains

Table 3.8: Cell lines and strains

Cell line/strain	Source
E.coli XL-10 competent cells	New England Biolabs
HEK293 6E cells	National Research Council of Canada [41]
Nur77 Jurkat reporter cells	Children's Cancer Research Institute (CCRI)

3.1.7 Software

Table 3.9: Software programs used for data analysis, illustrations and graphic design

Software	Company
PEAQ-DSC analysis software	Malvern Panalytical
Astra	Cesbo Ltd.
LabSolutions	Shimadzu Corporation
ProtParam online tool	Expasy
FlowJo Version 10	FlowJo LLC.
Microsoft Excel for Windows 2010	Microsoft
Inkscape	Inkscape Project

3.1.8 Miscellaneous material

Table 3.10: Miscellaneous material

Material	Manufacturer
Nuclease-free water	Thermo Scientific
gWiz plasmid	Sigma-Aldrich
Kanamycin sulfate	Sigma-Aldrich
Desoxyribonucleotide triphosphates (dNTP's)	Biozym
Agarose	Biozym
100bp DNA Ladder	New England Biolabs
GeneRuler 1kb Plus DNA Ladder	Thermo Scientific
SYBR safe	Thermo Scientific
Dialysis tubing	Sigma-Aldrich
TALON metal affinity resin	Takara
Trypan Blue solution	Sigma-Aldrich
Fuchs-Rosenthal Counting Chamber	Thermo Scientific
Precision Plus Protein Unstained Protein Standards	Bio-Rad
10x tris/glycine/SDS (TGS) buffer	Bio-Rad
Tris-acetate-edta (TAE) buffer	Thermo Scientific
Mini-PROTEAN TGX Precast Protein Gels	Bio-Rad
4x Laemmli sample buffer	Bio-Rad
High-performance liquid chromatography (HPLC) tubes	Bruckner Analysentechnik
Superdex 75 Increase 10/300 GL	Cytiva
Syringe filters (0.22 µm)	Thermo Scientific
HSA 20%	Octapharma
CASYton solution	OMNI Life Science
HPLC standards: Bovine serum albumin (BSA), ovalbumin, myoglobin, cytochrome c	Sigma-Aldrich
Ethidium bromide	Thermo Scientific

3.1.9 Amino acid sequences of single chain variable fragments (scFvs)

In Table 3.11 the selection of scFvs are listed. The table informs about the scFvs' binding targets and the amino acid sequences for V_L and V_H (including the sequence references). For the applied scFv design, see Figure 4.1 in chapter 4.2. The DNA sequences of the scFv constructs were ordered as clonal genes from TWIST bioscience. For all DNA sequences, codon optimization was performed using the codon usage of Homo sapiens.

Table 3.11: Amino acid sequences of scFvs (V_H and V_L)

Code	Name	Target	Reference
1	FMC63 scFv	CD19	doi: 10.1016/s0161-5890(97)00144-2
V_H sequence EVKLQESGPGLVAPSQSLSVTCTVSGVSLPDYGVSWIRQPPRKGLEWLGVIWGSETTYYNSALKSRLTIIKDNSKSQVFLK MNSLQTDDTAIYYCAKHYYYGGSYAMDYWGQGTSVTVSS **V_L sequence** DIQMTQTTSSLSASLGDRVTISCRASQDISKYLNWYQQKPDGTVKLLIYHTSRLHSGVPSRFSGSGSGTDYSLTISNLEQED IATYFCQQGNTLPYTFGGGTKLEIT			
2	14g2a scFv	GD2	Publication No.: KR20180104146A
V_H sequence EVQLLQSGPELEKPGASVMISCKASGSSFTGYNMNWVRQNIGKSLEWIGAIDPYYGGTSYNQKFKGRATLTVDKSSSTAYMH LKSLTSEDSAVYYCVSGMEYWGQGTSVTVSS **V_L sequence** DVVMTQTPLSLPVSLGDQASISCRSSQSLVHRNGNTYLHWYLQKPGQSPKLLIHKVSNRFSGVPDRFSGSGSGTDFTLKISR VEAEDLGVYFCSQSTHVPPLTFGAGTKLEL			
3	14g2a-E101K scFv	GD2	doi: 10.1158/2326-6066.CIR-17-0211
V_H sequence EVQLLQSGPELEKPGASVMISCKASGSSFTGYNMNWVRQNIGKSLEWIGAIDPYYGGTSYNQKFKGRATLTVDKSSSTAYMH LKSLTSEDSAVYYCVSGMKYWGQGTSVTVSS **V_L sequence** DVVMTQTPLSLPVSLGDQASISCRSSQSLVHRNGNTYLHWYLQKPGQSPKLLIHKVSNRFSGVPDRFSGSGSGTDFTLKISR VEAEDLGVYFCSQSTHVPPLTFGAGTKLEL			
4	HA22 scFv	CD22	doi: 10.1074/jbc.M409783200, PMID: 11948105
V_H sequence EVQLVESGGGLVKPGGSLKLSCAASGFAFSTYDMSWVRQTPEKRLEWVAYISSGGGTTYYPDTVKGRFTISRDNAKNTLYLQ MSSLKSEDTAMYYCARHSGYGTHWGVLFAYWGQGTLVTVSA **V_L sequence** DIQMTQTTSSLSASLGDRVTISCRASQDISNYLNWYQQKPDGTVKLLIYYTSILHSGVPSRFSGSGSGTDYSLTISNLEQED FATYFCQQGNTLPWTFGGGTKLEIK			
5	m971 scFv	CD22	Publication No.: US20190292238A1
V_H sequence QVQLQQSGPGLVKPSQTLSLTCAISGDSVSSNSAAWNWIRQSPSRGLEWLGRTYYRSKWYNDYAVSVKSRITINPDTSKNQF SLQLNSVTPEDTAVYYCAREVTGDLEDAFDIWGQGTMVTVSS **V_L sequence** DIQMTQSPSSLSASVGDRVTITCRASQTIWSYLNWYQQRPGKAPNLLIYAASSLQSGVPSRFSGRGSGTDFTLTISSLQAEDF ATYYCQQSYSIPQTFGQGTKLEIK			
6	Lenzilumab scFv	GM-CSF	doi: 10.1073/pnas.1616408114
V_H sequence QVQLVQSGAEVKKPGASVKVSCKASGYSFTNYYIHWVRQAPGQRLEWMGWINAGNGNTKYSQKFQGRVTITRDTSASTAYMEL SSLRSEDTAVYYCVRRQRFPYYFDYWGQGTLVTVSS **V_L sequence** EIVLTQSPATLSVSPGERATLSCRASQSVGTNVAWYQQKPGQAPRVLIYSTSSRATGITDRFSGSGSGTDFTLTISRLEPED FAVYYCQQFNKSPLTFGGGTKVEIK			

Table 3.11: Amino acid sequences of scFvs (V_H and V_L)

Code	Name	Target	Reference
7	Bococizumab scFv	PCSK9i	doi: 10.1073/pnas.1616408114
V_H sequence			
QVQLVQSGAEVKKPGASVKVSCKASGYTFTSYYMHWVRQAPGQGLEWMGEISPFGGRTNYNEKFKSRVTMTRDTSTSTVYMEL SSLRSEDTAVYYCARERPLYASDLWGQGTTVTVSS			
V_L sequence			
DIQMTQSPSSLSASVGDRVTITCRASQGISSALAWYQQKPGKAPKLLIYSASYRYTGVPSRFSGSGSGTDFTFTISSLQPEDI ATYYCQQRYSLWRTFGQGTKLEIK			
8	Sirukumab scFv	IL-6	doi: 10.1073/pnas.1616408114
V_H sequence			
EVQLVESGGGLVQPGGSLRLSCAASGFTFSPFAMSWVRQAPGKGLEWVAKISPGGSWTYYSDTVTGRFTISRDNAKNSLYLQMN SLRAEDTAVYYCARQLWGYYALDIWGQGTTVTVSS			
V_L sequence			
EIVLTQSPATLSLSPGERATLSCSASISVSYMYWYQQKPGQAPRLLIYDMSNLASGIPARFSGSGSGTDFTLTISSLEPEDFAV YYCMQWSGYPYTFGGGTKVEIK			
9	Glembatumumab scFv	Transmembrane glyoprotein NMB	doi: 10.1073/pnas.1616408114
V_H sequence			
QVQLVQSGAEVKKPGSSVKVSCKASGYSFTDYHIHWVRQAPGQGLEWMGVINPMYGTTDYNQRFKGRVTITADESTSTAYMELS SLRSEDTAVYYCARYDYFTGTGVYWGQGTLVTVSS			
V_L sequence			
EIVMTQSPATLSVSPGERATLSCRASQSVDNNLVWYQQKPGQAPRLLIYGASTRATGIPARFSGSGSGTEFTLTISSLQSEDF AVYYCQQYNNWPPWTFGQGTKVEIK			
10	Ixekizumab scFv	IL-17A	doi: 10.1073/pnas.1616408114
V_H sequence			
EVQLVESGGGLVQPGGSLRLSCAASGFNIKDTYIHWVRQAPGKGLEWVARIYPTNGYTRYADSVKGRFTISADTSKNTAYLQM NSLRAEDTAVYYCSRWGGDGFYAMDYWGQGTLVTVSS			
V_L sequence			
DIVMTQTPLSLSVTPGQPASISCRSSRSLVHSRGNTYLHWYLQKPGQSPQLLIYKVSNRFIGVPDRFSGSGSGTDFTLKISRVE AEDVGVYYCSQSTHLPFTFGQGTKLEIK			
11	Trastuzumab scFv	Her2	doi: 10.1073/pnas.1616408114
V_H sequence			
EVQLVESGGGLVQPGGSLRLSCAASGFNIKDTYIHWVRQAPGKGLEWVARIYPTNGYTRYADSVKGRFTISADTSKNTAYLQM NSLRAEDTAVYYCSRWGGDGFYAMDYWGQGTLVTVSS			
V_L sequence			
DIQMTQSPSSLSASVGDRVTITCRASQDVNTAVAWYQQKPGKAPKLLIYSASFLYSGVPSRFSGSRSGTDFTLTISSLQPEDF ATYYCQQHYTTPPTFGQGTKVEIK			
12	Tovetumab scFv	RTK: PDGFRA	doi: 10.1073/pnas.1616408114
V_H sequence			
QVQLVESGGGLVKPGGSLRLSCAASGFTFSDYYMNWIRQAPGKGLEWVSYISSSGSIIYYADSVKGRFTISRDNAKNSLYLQMN SLRAEDTAVYYCAREGRIAARGMDVWGQGTTVTVSS			
V_L sequence			
DIQMTQSPSSLSASVGDRVSITCRPSQSFSRYINWYQQKPGKAPKLLIHAASSLVGGVPSRFSGSGSGTDFTLTISSLQPEDF ATYYCQQTYSNPPITFGQGTRLEMK			

Table 3.11: Amino acid sequences of scFvs (V_H and V_L)

Code	Name	Target	Reference
13	Secukinumab scFv	IL-17A	doi: 10.1073/pnas.1616408114
V_H sequence			
EVQLVESGGGLVQPGGSLRLSCAASGFTFSNYWMNWVRQAPGKGLEWVAAINQDGSEKYYVGSVKGRFTISRDNAKNSLYLQM NSLRVEDTAVYYCVRDYYDILTDYYIHYWYFDLWGRGTLVTVSS			
V_L sequence			
EIVLTQSPGTLSLSPGERATLSCRASQSVSSSYLAWYQQKPGQAPRLLIYGASSRATGIPDRFSGSGSGTDFTLTISRLEPEDF AVYYCQQYGSSPCTFGQGTRLEIK			
14	Cetuximab scFv	EGFR	doi: 10.1073/pnas.1616408114
V_H sequence			
QVQLKQSGPGLVQPSQSLSITCTVSGFSLTNYGVHWVRQSPGKGLEWLGVIWSGGNTDYNTPFTSRLSINKDNSKSQVFFKMN SLQSNDTAIYYCARALTYYDYEFAYWGQGTLVTVSA			
V_L sequence			
DILLTQSPVILSVSPGERVSFSCRASQSIGTNIHWYQQRTNGSPRLLIKYASESISGIPSRFSGSGSGTDFTLSINSVESEDI ADYYCQQNNNWPTTFGAGTKLELK			
15	Dinutuximab scFv	GD2	doi: 10.1073/pnas.1616408114
V_H sequence			
EVQLLQSGPELEKPGASVMISCKASGSSFTGYNMNWVRQNIGKSLEWIGAIDPYYGGTSYNQKFKGRATLTVDKSSSTAYMHLK SLTSEDSAVYYCVSGMEYWGQGTSVTVSS			
V_L sequence			
EIVMTQSPATLSVSPGERATLSCRSSQSLVHRNGNTYLHWYLQKPGQSPKLLIHKVSNRFSGVPDRFSGSGSGTDFTLKISRV EAEDLGVYFCSQSTHVPPLTFGAGTKLELK			
16	Epratuzumab scFv	CD22	doi: 10.1073/pnas.1616408114
V_H sequence			
QVQLVQSGAEVKKPGSSVKVSCKASGYTFTSYWLHWVRQAPGQGLEWIGYINPRNDYTEYNQNFKDKATITADESTNTAYMEL SSLRSEDTAFYFCARRDITTFYWGQGTTVTVSS			
V_L sequence			
DIQLTQSPSSLSASVGDRVTMSCKSSQSVLYSANHKNYLAWYQQKPGKAPKLLIYWASTRESGVPSRFSGSGSGTDFTFTISS LQPEDIATYYCHQYLSSWTFGGGTKLEIK			

3.1.10 DNA sequences of the chimeric antigen receptor (CAR) backbone elements

The design of the CAR constructs is illustrated in chapter 4.2. Table 3.12 lists the respective DNA sequences of the CAR elements. The template of the CAR backbone was provided by Benjamin Salzer (CCRI, Vienna).

Table 3.12: DNA sequences of the CAR backbone elements

CAR element	DNA sequence
CD28 stalk region	CCTAGCCCACTGTTCCCCGGGCCTTCCAAGCCT
CD28 transmembrane region	TTCTGGGTCTTAGTCGTCGTGGGGGGCGTGTTAGCGTGTTACTC GCTCTTGGTCACCGTCGCGTTCATAATATTTTGGGTC
CD28 co-stimulatory domain	CGCTCGAAACGCTCGCGCTTGTTACATTCGGATTATATGAATATG ACGCCGAGGAGGCCGGGCCCGACGAGGAAACACTATCAACCGTA CGCGCCCCCCAGGGATTTTGCCGCGTACAGGAGT
CD3ζ domain	TTACGCGTCAAATTTTCGCGCTCGGCCGATGCGCCGGCCTATCAA CAAGGGCAAAATCAATTGTACAATGAATTGAACTTGGGCAGGCG CGAAGAATATGACGTGCTCGATAAACGCAGGGGGAGAGATCCGG AAATGGGCGGCAAACCCCGCCGCAAAAATCCGCAAGAGGGGTTA TATAACGAGTTACAAAAGGACAAAATGGCCGAAGCGTATTCGGA AATAGGCATGAAGGGGGAAAGGAGACGCGGGAAAGGCCATGACG GGTTGTATCAAGGGTTGTCCACCGCGACGAAAGATACGTATGAT GCGTTGCATATGCAAGCGTTACCGCCGAGG

3.1.11 Primer sequences

Primers were ordered from Sigma-Aldrich or Microsynth. Amplification primers for scFv sequences are listed in Table 3.13. Amplification primers for CAR sequences (1st step polymerase chain reaction (PCR) and 2nd step PCR) are listed in Tables 3.14 and 3.15. Table 3.16 and Table 3.17 show the primers used for sequencing of scFv DNA sequences and CAR DNA sequences, respectively.

Table 3.13: Primers for amplification of scFv-coding DNA. The bases written in capital letters match the template sequences. The bases written in lowercase are part of the gWiz vector sequence and form the overhangs required for scFv-vector assembly.

Primer	Sequence
scFv_fwd	5‘–cacgtgtgatcagatatcgcGCCACCATGGAGTTGGGG–3’
scFv_fwd1	5‘–cacgtgtgatcagatatcgcGCCACCATGGAATTGGGG–3’
scFv_fwd2	5‘–cacgtgtgatcagatatcgcGCCACCATGGAGCTCGGG–3’
scFv_fwd3	5‘–cacgtgtgatcagatatcgcGCCACCATGGAGCTGGGT–3’
scFv_fwd4	5’–cacgtgtgatcagatatcgcGCCACCATGGAGCTTGGA–3’
scFv_fwd5	5’–cacgtgtgatcagatatcgcGCCACCATGGAGCTGGGG–3’
scFv_fwd6	5’–cacgtgtgatcagatatcgcGCCACCATGGAACTGGGA–3’
scFv_fwd7	5’–cacgtgtgatcagatatcgcGCCACCATGGAACTGGGG–3’
scFv_fwd8	5’–cacgtgtgatcagatatcgcGCCACCATGGAACTCGGG–3’
scFv_fwd9	5‘–cacgtgtgatcagatatcgcGCCACCATGGAGTTGGGC–3’
scFv_rev	5‘–tattagccagaagtgatctgTTATTAGTGATGATGGTGGTGGTGG–3’
scFv_rev1	5‘–tattagccagaagtgatctgTTATTAGTGATGATGGTGGTGGTGA–3’
scFv_rev2	5‘–tattagccagaagtgatctgTTATTAATGATGGTGATGGTGGTGGTGG–3’
scFv_rev3	5‘–tattagccagaagtgatctgTTATTAATGGTGATGGTGATGATGGTGG–3’
scFv_rev4	5‘–tattagccagaagtgatctgTTATTAATGGTGGTGATGATGGTGATGA–3’
scFv_rev5	5‘–tattagccagaagtgatctgTTATTAGTGATGGTGATGATGATGGTG–3’
scFv_rev6	5‘–tattagccagaagtgatctgTTATTAGTGATGGTGATGGTGGTGA–3’
scFv_rev7	5‘–tattagccagaagtgatctgTTATTAATGGTGGTGGTGATGGTGA–3’
scFv_rev8	5‘–tattagccagaagtgatctgTTATTAGTGATGGTGGTGATGATGG–3’
scFv_rev9	5‘–tattagccagaagtgatctgTTATTAGTGATGGTGATGATGGTGGTG–3’
scFv_rev10	5‘–tattagccagaagtgatctgTTATTAGTGGTGATGATGATGATGGTG–3’
scFv_rev11	5‘–tattagccagaagtgatctgTTATTAGTGGTGGTGGTGATGATGG–3’
scFv_rev12	5‘–tattagccagaagtgatctgTTATTAGTGATGGTGGTGGTGGTGG–3’
scFv_rev13	5‘–tattagccagaagtgatctgTTATTAGTGGTGGTGGTGGTGATGG–3’
scFv_rev14	5‘–tattagccagaagtgatctgTTATTAGTGATGGTGGTGATGGTGG–3’

Table 3.14: Primers for amplification of CAR-coding DNA (1st step PCR). The bases written in capital letters match the template sequences. Bases written in lowercase letters indicate overhangs.

Primer	Sequence
Fwd1	5‘–tcgtttagtgaaccgtcagtaatacgactcactatagggactcaGCCACCATGGAGCTTGGACT–3’
Fwd2	5‘–tcgtttagtgaaccgtcagtaatacgactcactatagggactcaGCCACCATGGAGCTGGGTCT–3’
Fwd3	5‘–tcgtttagtgaaccgtcagtaatacgactcactatagggactcaGCCACCATGGAACTGGGACT–3’
Fwd4	5‘–tcgtttagtgaaccgtcagtaatacgactcactatagggactcaGCCACCATGGAGCTCGGGCT–3’
Fwd5	5‘–tcgtttagtgaaccgtcagtaatacgactcactatagggactcaGCCACCATGGAACTCGGGCT–3’
Fwd6	5‘–tcgtttagtgaaccgtcagtaatacgactcactatagggactcaGCCACCATGGAGTTGGGCCT–3’
Fwd7	5‘–tcgtttagtgaaccgtcagtaatacgactcactatagggactcaGCCACCATGGAGTTGGGGTT–3’
Fwd8	5‘–tcgtttagtgaaccgtcagtaatacgactcactatagggactcaGCCACCATGGAACTGGGGTT–3’
Fwd10	5‘–tcgtttagtgaaccgtcagtaatacgactcactatagggactcaGCCACCATGGAGCTGGGGCT–3’
Fwd11	5‘–tcgtttagtgaaccgtcagtaatacgactcactatagggactcaGCCACCATGGAGTTGGGCTT–3’
Rev_scFv1	5‘–cttgtcgtcatcgtctttgtagtcgctgcctcctcctccGGATCCTCCCCCTCCACT–3’
Rev_scFv2	5‘–cttgtcgtcatcgtctttgtagtcgctgcctcctcctccAGACCCGCCACCGCCGGA–3’
Rev_scFv3	5‘–cttgtcgtcatcgtctttgtagtcgctgcctcctcctccACTGCCTCCTCCCCCACT–3’
Rev_scFv4	5‘–cttgtcgtcatcgtctttgtagtcgctgcctcctcctccGGAGCCTCCACCGCCGGC–3’
Rev_scFv5	5‘–cttgtcgtcatcgtctttgtagtcgctgcctcctcctccAGATCCTCCCCCCCCGCT–3’
Rev_scFv6	5‘–cttgtcgtcatcgtctttgtagtcgctgcctcctcctccAGAGCCGCCTCCGCCGCT–3’
Rev_scFv7	5‘–cttgtcgtcatcgtctttgtagtcgctgcctcctcctccTGATCCTCCGCCTCCAGA–3’
Rev_scFv8	5‘–cttgtcgtcatcgtctttgtagtcgctgcctcctcctccTGAACCTCCTCCGCCGCT–3’
Rev_scFv9	5‘–cttgtcgtcatcgtctttgtagtcgctgcctcctcctccACTTCCCCCGCCGCCACT–3’
Rev_scFv10	5‘–cttgtcgtcatcgtctttgtagtcgctgcctcctcctccTGAGCCGCCCCCCCCAGA–3’
Rev_scFv11	5‘–cttgtcgtcatcgtctttgtagtcgctgcctcctcctccGGAGCCACCGCCCCCGCT–3’
Rev_scFv12	5‘–cttgtcgtcatcgtctttgtagtcgctgcctcctcctccTGACCCGCCGCCTCCTGA–3’
Rev_scFv13	5‘–cttgtcgtcatcgtctttgtagtcgctgcctcctcctccGGACCCTCCCCCTCCGCT–3’
Rev_scFv14	5‘–cttgtcgtcatcgtctttgtagtcgctgcctcctcctccGGAACCCCCGCCGCCCGC–3’
Rev_scFv15	5‘–cttgtcgtcatcgtctttgtagtcgctgcctcctcctccTGAGCCCCCTCCTCCGGA–3’
Rev_scFv16	5‘–cttgtcgtcatcgtctttgtagtcgctgcctcctcctccACTCCCACCCCCGCCGGA–3’
Fwd_backbone	5‘–gactacaaagacgatgacgacaagCCTAGCCCACTGTTCCCCG–3’
Rev_backbone	5‘–attcctgcagcccgtagttttaCCTCGGCGGTAACGCTTG–3’

Table 3.15: Primers for amplification of CAR-coding DNA (2nd step PCR)

Fwd_T7	5‘–CGTCAGTAATACGACTCACTATAGGGACTCAGCCACC–3’
Rev_backbone	5‘–CCCGTAGTTTTACCTCGGCGGTAACGCTTGCA–3’

Table 3.16: Sequencing primers for scFv DNA sequences

Fwd_gWiz	5‘–GGAGGGCAGTGTAGTCTGAG–3‘
Rev_gWiz	5‘–TCAAGGAAGGCACGGGGGA–3‘

Table 3.17: Sequencing primers for CAR DNA sequences

Fwd_CAR_seq	5‘–CGACTCACTATAGGGACTCA–3‘
Rev_CAR_seq	5‘–TTACCTCGGCGGTAACG–3‘

3.2 Methods

3.2.1 Molecular biology methods

3.2.1.1 PCR

All PCR reactions were performed with the Q5 Hot Start High-Fidelity DNA Polymerase from New England Biolabs. For all PCR reactions, 50 µL setups were prepared (Table 3.18). The PCR conditions listed in Table 3.19 were applied for scFv DNA amplification for soluble expression

and the 1st step PCR reactions of CAR cloning (Section 3.2.2.2). For these reactions, a final template concentration of 10 ng/µL was used. For the 2nd step PCR reactions in the CAR cloning process, the protocol was modified as follows: The annealing step was shortened to 30 seconds and the final extension step was shortened to two minutes. In terms of the PCR reaction setup only 0.5 µL of template DNA (Gibson-assembled CAR) were used. The amplified DNA was analyzed with agarose gel electrophoresis. PCR products were purified using the Monarch PCR & DNA cleanup kit. Purified DNA was stored at -20°C.

Table 3.18: General PCR reaction setup

Component	**Volume**
5x Q5 Reaction Buffer	10 µL
10 mM dNTP's	1 µL
10 µM Forward primer	2.5 µL
10 µM Reverse primer	2.5 µL
Template DNA	1 µL
Q5 High-Fidelity DNA Polymerase	0.5 µL
Nuclease-free water to	50 µL

Table 3.19: General PCR cycle conditions

Step	**Temperature**	**Time**
Initial denaturation	98°C	0:30
Denaturation	98°C	0:10
Annealing	XX°C	1:00
Extension	72°C	1:00
Final extension	72°C	10:00
End	4°C	∞
XX = respective primer annealing temperature For all PCR reactions, 25 cycles were applied		

3.2.1.2 Restriction digest

For restriction digests, 4-20 U of the corresponding restriction enzyme were used for 1-2 µg of vector DNA in 50 µL setups. The reactions were incubated at 37°C for 1-2 hours.

3.2.1.3 HiFi DNA Assembly

For assembly of DNA fragments, the NEBuilder HiFi DNA Assembly Master Mix was used. The molar ratio of vector to insert for scFv-plasmid ligations was chosen according to the manufacturer's recommendation for two fragments (Table 3.20). For cloning of the CAR constructs, the applied molar ratio of scFv fragment to CAR backbone fragment was 1:1. A HiFi DNA assembly setup is summarized in Table 3.21 . The volumes of vector and insert DNA corresponding to the moles in Table 3.21 depended on the DNA concentrations and the construct lengths. For mole to mass conversion, the New England Biolabs online calculator was used.

3.2.1.4 Agarose gel electrophoresis

Analytical agarose gels were prepared with 1% (w/v) agarose. For analytical gels, 1.2 g agarose were dissolved in 120 mL of TAE buffer. For preparative gels, 1.5 g agarose and 150 mL TAE

Table 3.20: HiFi DNA Assembly – recommended amounts of fragments according to manufacturer protocol

DNA molar ratio (vector:insert)	**1:2**
Vector amount	0.028 pmol
scFv DNA amount	0.056 pmol

Table 3.21: HiFi DNA Assembly – reaction setup

Component	**Volume**
Fragment 1 (vector/backbone)	x µL
Fragment 2 (scFv DNA)	y µL
HiFi DNA Assembly Master Mix	5 µL
Deionized water	5 – x – y µL
Final volume	10 µL

buffer were used. The mixture was heated in the microwave for approximately 1 minute using high power settings. The agarose solution was left to cool down and was subsequently poured into a cast. In the cast and while still liquid, the respective volume of SYBR safe DNA gel stain (10000x) was added. The solidified gel was placed in an electrophoresis chamber and fully immersed in TAE buffer. Prior to loading, samples were mixed with gel loading dye. As a size reference, either the 100bp DNA Ladder from New England Biolabs or the GeneRuler 1kb Plus DNA Ladder from ThermoScientific was loaded. Once all samples were loaded, a voltage of 120 V was applied and the gel was run for approx. 45 minutes. The loading volumes were 6 µL for analytical gels and up to 55 µL for preparative gels. The gels were imaged with the Gel Dox XR+ Gel Documentation System from Bio-Rad.

3.2.1.5 Heat shock transformation

For the transformation of chemically competent cells with plasmids, a heat shock transformation was performed. 25 µL aliquots of heat-shock competent cells were thawed on ice and subsequently mixed with 2 µL of diluted plasmid DNA resulting in a final plasmid amount of 2-10 ng per reaction. The reaction was mixed gently by snipping and incubated on ice for 20 minutes. Afterwards, the cells were heat-shocked for 45 seconds at 42°C. Then the cells were transferred on ice again for 2 minutes and 0.5 mL pre-warmed, antibiotic-free LB-medium were added. The cells were incubated under shaking (300 rpm) at 37°C for 40 minutes. Finally, the transformed cells were plated on LB-agar plates, containing Kanamycin, using sterile glass beads and the plates were incubated at 37°C overnight.

3.2.1.6 SDS PAGE

For SDS PAGE, stain-free precast gels were used. 15 µL of sample were mixed with 5 µL 4x Laemmli buffer and heated at 95°C for 5 minutes. The loading volume per sample was 15 µL. The loading volume of the unstained protein standard was 8 µL. Concentrated samples were diluted to load approximately 5-10 µg of protein per well. The samples were run at 180 V for approximately 25 minutes. The gels were imaged with the Gel Dox XR+ Gel Documentation System from Bio-Rad.

3.2.1.7 Cryo stocks

For the preparation of cryo stocks, 714 µL of E.coli overnight culture were added to 286 µL of 70% glycerol in a 2 mL cryo tube. The resulting glycerol concentration was 20%. Cryo stocks

were stored at -80°C.

3.2.2 Cloning methods

3.2.2.1 Cloning of soluble scFvs

After successful PCR amplification with the primers described in Table 3.13, the purified scFv sequences were Gibson-assembled with a double-digested gWiz vector. The digest was carried out with the high-fidelity restriction enzymes BamHl-HF and Notl-HF from New England Biolabs. The success of the digestion was analyzed with an analytical agarose gel electrophoresis. The scFv-containing plasmids were introduced into competent XL-10 cells via heat shock transformation. The following day, clones were picked, and overnight cultures were set up for subsequent plasmid isolation using the Monarch plasmid miniprep kit (New England Biolabs). For sequence verification of the inserts, the plasmids were sent to sequencing (Mycrosynth) using the gWiz sequencing primers (Table 3.16). Cryo stocks were prepared of clones containing sequence-verified plasmids.

3.2.2.2 Cloning of CARs

In a first step the scFv part and the CAR backbone were PCR-amplified (=1st step PCR). In this PCR step a T7 promotor sequence overhang was introduced at the scFv 5'-end. At the scFv 3'-end and the CAR backbone 5'-end, overhangs of an additional 1xG4S linker and a FLAG-tag sequence were introduced (Figure 3.1). For elimination of template DNA, the PCR products were subjected to a Dpnl restriction digest using 4U enzyme for 1 µg DNA. Subsequently, PCR products were purified using the Monarch Genomic DNA purification kit (New England Biolabs) and the amplified scFv and CAR backbone sequences were assembled using the NEBuilder HiFi DNA Assembly Master Mix (New England Biolabs). The assembled CAR DNA was then amplified in a second PCR (=2nd step PCR). The 2nd step PCR products were loaded onto a preparative agarose gel and the DNA bands at the expected height for the CAR DNA were excised and purified using the Monarch DNA gel extraction kit (New England Biolabs). Samples of the purified CAR DNA sequences were sent to sequencing (Mycrosynth). The sequence-verified CAR DNA sequences were used as templates for *in vitro* transcription.

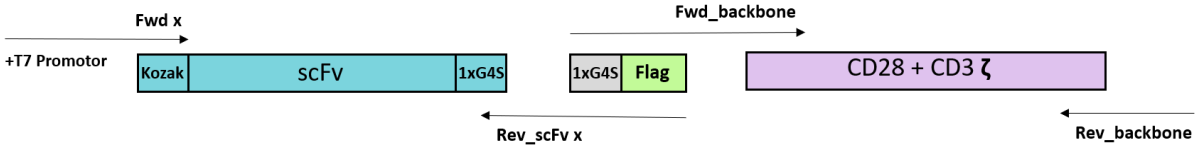

Figure 3.1: CAR cloning strategy – arrows indicate primers used in 1st step PCR

3.2.3 Cell biology methods

3.2.3.1 Cultivation of HEK293 6E cells

HEK293 6E cells were cultivated in suspension using Freestyle F17 medium from Gibco supplemented with L-glutamine (4mM), G418 (25 µg/mL) and pluronic (0.1%). Culture flasks had vented caps and were filled to no more than a fifth of their capacity to ensure proper aeration. The cultures were incubated at 37°C and 8% CO_2. The cells were cultured with a density between 0.25 x 10^6 and 2 x 10^6 cells/mL. To keep them within this range, cells were passaged every two to three days. The cell count was determined with a Fuchs-Rosenthal counting chamber. Typically, 100 µL of cell suspension were diluted with 450 µL of PBS and mixed with 50 µL trypan blue. 20 µL of this mixture were pipetted into the chamber and minimum four large squares were counted

under the light microscope. For the calculation of the number of cells/mL, the following formula was used:

$$\text{cell density } (\tfrac{cells}{mL}) = \text{average cell count per large square} \times \text{dilution factor} \times 5000$$

The factor 5000 is required for extrapolation of the counted volume (0.2 mm^3) to 1 mL.

3.2.3.2 Cultivation of Nur77 Jurkat reporter cells

Nur77 Jurkat cells were cultivated in RPMI medium supplemented with 10 % FBS and 1 % P/S. Cells were cultured with a density between 0.2 x 10^6 cells/mL and 2 x 10^6 cells/mL. Cells were passaged every two to three days and incubated at 37°C and 5% CO_2. Jurkat cells were counted using a CASY cell counter.

3.2.3.3 Transient transfection of HEK293 6E cells

The desired cell density for transfection was 1.5-2 x 10^6 cells/mL. Cells were splitted one day prior to transfection to a density of 1.0 x 10^6 cells/mL. The cationic polymer PEI was used as vehicle for DNA transfer into HEK cells. For DNA preparation, a 200 mL overnight culture of the respective E.*coli* clone was set up and plasmids were purified the following day with the NucleoBond Xtra Midi kit (Macherey Nagel). Concentrations usually ranged from 2.5-8 mg/mL. The applied ratio of PEI:DNA was 2.5:1. The PEI stock solution had a concentration of 1 mg/mL. The desired end concentrations of DNA and PEI were 1 µg/mL and 2.5 µg/mL and the required volumes of DNA and PEI stock solutions were diluted in 0.5 or 0.75 mL pre-warmed medium, respectively. After three minutes of incubation at room temperature, the PEI-medium solution was slowly added to the DNA-medium solution under constant, gentle mixing. Once combined, the PEI-DNA mixture was incubated at room temperature for 10 minutes. Finally, the PEI-DNA complex solution was added dropwise to the cell culture flask under constant shaking. The transfected cells were again incubated. To enhance the cell's productivity, 48 hours post transfection, the cells were fed with TN1-solution and glucose solution resulting in final concentrations of 0.5% and 0.25%, respectively. Cells were harvested five days after transfection.

3.2.4 Harvest, dialysis and purification of soluble scFvs

3.2.4.1 Harvest

First, the HEK cell suspension was centrifuged at 500g (15 minutes, 4°C) to separate cells from the supernatant. The cell pellet was discarded and the supernatant was subjected to a second centrifugation step at 15000g (15 minutes, 4°C) to remove cell debris.

3.2.4.2 Buffer exchange

For buffer exchange, the HEK supernatants were dialyzed in TALON equilibration buffer overnight at 4°C. For 50 mL supernatant, 5 L buffer were used. The supernatants were filled in dialysis tubings (MWCO 12400, Sigma-Aldrich) and placed in the beakers filled with buffer applying gentle stirring.

3.2.4.3 Purification

Once dialyzed, the His-tagged scFvs were purified via immobilized metal affinity chromatography (IMAC) using HisTALON gravity flow glass columns and TALON metal affinity resin. For one purification, 1.5-2 mL resin were used. The resin was filled into the glass column, washed with RO water (2x20 mL) and equilibrated with equilibration buffer (1x20 mL). Prior to sample loading, imidazole was added to the sample to a final concentration of 10 mM to avoid unspecific

binding to the column. The sample was loaded onto the column twice. After two washing steps with wash buffer 1 and 2 (20 mL each), the sample was eluted with 2x5 mL elution buffer. The column was cleaned with regeneration buffer, RO water and 20% ethanol. The resin was stored in 20% ethanol at 4°C. Resins were re-used for purification of the same scFvs. The purified proteins were buffer-exchanged to 1xPBS and concentrated to a final volume under 1.5 mL using Amicon Ultra-15 10K centrifugal filters. Protein concentrations were determined with a DeNovix spectrophotometer. The scFv's extinction coefficients and molecular weights (Mws) used for the concentration determination were calculated with the ProtParam online tool and are listed in Table 3.22. The purified and concentrated proteins were stored at -80°C.

Table 3.22: Extinction coefficients and molecular weights of solubly expressed scFvs determined with the ProtParam online tool

scFv	**Exctinction coefficient(M^{-1} cm^{-1})**	**Mw (Da)**
FMC63 scFv	51590	27914
m971 scFv	56630	28420
Sirukumab scFv	61100	27389
Trastuzumab scFv	50100	27775
Tovetumab scFv	41620	27715
Secukinumab scFv	60070	29007
Cetuximab scFv	51130	27818
Dinutuximab scFv	38640	27526

3.2.5 Construction of chimeric antigen receptors

The CAR DNA constructs were equipped with a T7 promotor sequence (TAATACGACTCACTATAGGG) at the 5' end to allow for the preparation of CAR mRNAs by *in vitro* transcription. This sequence was followed by the scFv portion consisting of a Kozak sequence (GCCACC), an Ig heavy chain signal peptide, the V_L domain, a Whitlow linker (18aa) and the V_H domain. A 2xG4S linker was used to connect the scFv part with a FLAG-tag sequence (used for CAR expression detection) and the CAR backbone consisting of the CD28 stalk region, the CD28 transmembrane region, the CD28 co-stimulatory domain and the CD3ζ activation domain. For amino acid sequences of the V_H and V_L domains, see Table 3.11. For DNA sequences of CAR backbone elements, see Table 3.12. The scFv and CAR designs are illustrated in chapter 4 (Figures 4.1 and 4.2).

3.2.5.1 *In vitro* transcription

The sequence-verified CAR constructs (=purified 2^{nd} step PCR products) were used as templates for *in vitro* transcription. For this purpose, the mMessage mMachine T7 Ultra Kit was used. The reactions were carried out according to manufacturer protocol except for a prolonged incubation time of 1.5 hours and a reduced reaction volume of 10 µL. The amounts of used template ranged between 0.1-0.2 µg. Before and after poly A tailing, samples were taken for agarose gel electrophoresis analysis.

3.2.5.2 mRNA purification

For purification of *in vitro* transcribed mRNA, an adapted protocol from the RNeasy Kit (QIAGEN) was applied. For each purification setup, 375 µL RLT buffer from the kit were mixed with 1% beta-mercaptoethanol. Then 275 µL absolute ethanol were added and the tube was snipped for mixing. The mixture was loaded onto the provided column and subsequent steps were carried out according to manufacturer protocol. Once purified, the mRNA concentrations

were determined with a DeNovix spectrophotometer and aliquoted to 5 µg. The aliquots were frozen at -80°C until they were used for mRNA electroporation of Jurkat reporter cells.

3.2.6 mRNA electroporation

For the introduction of mRNA into Jurkat reporter cells, mRNA electroporation was performed. Jurkat reporter cells were counted using a CASY cell counter. Aiming for a final cell number of 0.5 to 1 Mio electroporated cells for each condition and assuming that approximately 50% of the electroporated cells will die, for each condition 1 to 2 Mio cells were spun down in a tube (450 g, 5 minutes, RT) and the supernatant was discarded. Cell pellets where then subject to three washing steps using 15-20 mL of each: RPMI (containing phenolred), RPMI (phenol-free) and Opti-MEM. After the last washing step all supernatant was removed and cells were resuspended in 100 µL Opti-MEM. Subsequently, the mRNA (5 µg) was pipetted in the bottom of the electroporation cuvette (gap width: 4 mm) and cells were added on top. After gentle mixing by snipping, the cuvette was placed in the electroporator and pulsed applying the Gene Pulser square wave protocol (500 V, 3 ms, 4 mm cuvette). Electroporated cells were immediately transferred into an appropriate volume of fresh pre-warmed medium to reach a final cell density of 0.3 to 0.5 x 10^6/mL. The cells were incubated at 37°C for approximately 16-20 h before they were used for experiments.

3.2.7 Experimental methods

3.2.7.1 Differential scanning calorimetry (DSC)

For DSC experiments, samples were thawed and centrifuged (15000 rpm, 10 minutes, 4°C) to remove any precipitates. 325 µL of each sample (10 µM) were heated up from 20-100°C with a heating rate of 1°C/min. Prior to sample measurements, five buffer runs were performed. After buffer baseline subtraction, the curves were fitted with a non-two-state fitting model and the T_{m} was determined. Measurements were carried out with the PEAQ-DSC Automated system from Malvern Analytical.

3.2.7.2 Size-exclusion chromatography (SEC)-multiangle light scattering (MALS)

The scFv samples were thawed and centrifuged (15000 rpm, 10 minutes, 4°C) to remove any precipitates. The samples were diluted with SEC running buffer (1xPBS, 200 mM NaCl), if necessary, aiming at a final concentration of 0.2 µg/µL. Subsequently, 20 µg of the proteins were transferred into HPLC tubes and applied on a Superdex 75 column (10 mm x 300 mm). The column was connected to a HPLC Prominence LC20 system and the proteins were eluted with a flow rate of 0.75 mL/min (25°C). The proteins were detected with the MALS Dawn 8+ detector from Wyatt and a UV/VIS Photodiode Array Detector (Shimadzu).

3.2.7.3 Flow cytometry

3.2.7.3.1 Nur77 Jurkat reporter cell line

For the determination of the tonic signaling behavior of the CAR constructs, a Nur77 Jurkat reporter cell line was used. This cell line was generated and kindly provided by Benjamin Salzer (CCRI, Vienna) by introducing a Nur77-mKusabiraOrange2(mKO2) fusion gene into a Jurkat cell line using the CRISPR/Cas9 system. Nur77 was chosen as reporter molecule because it is over-expressed upon antigen-specific stimulation of T cells. In contrast to the commonly used CD69 reporter, the overexpression of Nur77 seems to be specific for antigen receptor signaling [42].

3.2.7.3.2 Analysis of CAR expression (FLAG tag staining) and tonic signaling

For the analysis of the CAR expression and the CAR tonic signaling behavior, the Jurkat reporter cells were counted 16-20 hours after electroporation using a CASY cell counter. Subsequently, a total of 10^5 cells were transferred into FACS tubes. The collected cells were first washed with 1 mL FACS buffer. In all washing steps cells were centrifuged at 1600 rpm for 5 minutes at 4°C. The buffer was removed completely and 50 µL blocking solution (10% HSA in FACS buffer) were added to the cells. After vortexing, the cells were incubated in the blocking solution for 15 minutes at 4°C. Subsequently, 0.3 µL of the anti-FLAG antibody were added. Cells were vortexed and incubated for at least 30 minutes at 4°C. After two washing steps with FACS buffer, the cells were analyzed with a LSR Fortessa instrument.

Chapter 4

Results

4.1 Selection of the scFv candidates

To investigate whether biophysical characteristics of scFvs can be correlated with their influence on tonic signaling when used as CAR binding domains, we aimed to test a range of scFvs with different biophysical properties on identical CAR backbones. Subsequently, we sought to solubly express scFvs associated with noticeable tonic signaling behavior of respective CARs, to analyze their aggregation and nonspecific binding behavior. We hypothesized that scFvs would lead to tonic CAR signaling when they exhibit high nonspecific binding ('sticky' scFvs) or when scFvs show multimerization or higher aggregation tendencies.

Our main source for the scFv selection was an extensive dataset created within a large-scale analysis of the biophysical properties of 137 isotype matched IgG1 antibodies performed by the company Adimab (further referred to as 'Adimab study')[43]. Within this analysis the antibody isotypes where subject to a couple of different biophysical assays revealing the antibodies' nonspecific binding and aggregation behavior as well as their thermal stability. Due to the fact that these antibodies only differed in their variable regions, the differences in the assay performance can be assumed to be the result of the distinct intrinsic properties of the variable domains only. Hence, we assumed that scFvs consisting of the investigated variable domains would likewise perform good or bad in the respective assay. Therefore, this collection allowed us to identify a subset of scFvs which are prone to self- and cross-interactions as well as a subset of scFvs which exhibit little self- and cross-interactions. For simplicity, the former subset shall be referred to as sticky scFvs and the latter as non-sticky scFvs. In both cases, we included scFvs of high and low thermal stability. Thus, we selected scFvs that fulfill the following characteristics:

- non-sticky with a range of thermal stabilities
- sticky with a range of thermal stabilities

In a first step, a selection of sticky candidates was discovered by filtering for antibodies that fell under the 10% of worst performing antibodies (as described by Jain et al.) in multiple self- and cross-interaction assays as well as hydrophobic interaction assays. In a second step, a selection of non-sticky candidates were chosen by filtering for antibodies that performed well in the aforementioned assay types [43]. Subsequently, any candidates specific for antigens that are potentially present on the surface of Jurkat T cells were excluded from analysis to rule out target recognition among Jurkat reporter cells. The final selection consisted of candidates with the highest and lowest thermal stability within the groups of pre-selected sticky and non-sticky antibodies (Figure 6.1).

Additionally, we selected a couple of scFvs which are currently used in CARs. This subset of scFvs will be referred to as benchmark scFvs. The group of Long and colleagues has linked the 14g2a scFv with tonic CAR signaling. Therefore, the 14g2a scFv was included as positive control

for tonic signaling. Additionally, the group observed tonic activation in CARs incorporating the CD22-targeting scFvs HA22 and m971 (albeit to a lesser extent than with the 14g2a scFv). Thus, these two scFvs were included as well. Long et al. did not observe tonic signaling of CARs based on the clinically used FMC63 scFv targeting the antigen CD19 [34]. Therefore, the FMC63 scFv was included to serve as negative control for tonic signaling. Lastly, we included the 14g2a-E101K scFv in our set as it has been associated with severe CAR T cell exhaustion [40]. This scFv is an affinity-matured version of the 14g2a scFv which contains an E101K mutation in the CDR3 of the 14g2a-V_H domain [44]. Table 4.1 shows the final list of selected sticky and non-sticky candidates as well as benchmark scFvs, including the individual antigens they are targeting.

Table 4.1: Selection of scFvs for the analysis of the tonic signaling behavior of respective CARs – including the scFv target antigens.

ScFv	**Target**	
FMC63 scFv	CD19	benchmark scFvs
14g2a scFv	GD2	
14g2a-E101K scFv	GD2	
HA22 scFv	CD22	
m971 scFv	CD22	
Lenzilumab scFv	GM-CSF	sticky scFvs
Bococizumab scFv	PCSK9	
Sirukumab scFv	IL-6	
Glembatumumab scFv	NMB	
Ixekizumab scFv	IL-17A	
Trastuzumab scFv	Her2	non-sticky scFvs
Tovetumab scFv	RTK: PDGFRA	
Secukinumab scFv	IL-17A	
Cetuximab scFv	EGFR	
Dinutuximab scFv	GD2	
Epratuzumab scFv	CD22	

4.2 ScFv and CAR Design

The scFv and CAR designs were identical for all 16 constructs. The scFvs were designed in a V_L-V_H orientation. The domains were connected with a Whitlow linker which contains a proline residue and charged amino acids for increased proteolytic stability [24]. The long linker length of 18 amino acids provides the necessary length for correct domain pairing [22]. Upstream of the V_L domain a Ig heavy chain signal peptide (SP) was included for scFv secretion (H1 from [45]). For soluble expression of selected scFvs, a 8xHis tag (8H) was attached at the C-terminus of the V_H domain using a 1xG4S linker (Figure 4.1).

For the tonic signaling analysis, the scFv sequences (lacking the 1xG4S linker and the His tag) were fused to identical CAR backbones (Figure 4.2). Given the report of tonic signaling augmentation upon CD28 co-stimulation, the CD28 co-stimulatory domain was included in the CAR design together with the CD28 transmembrane region and the CD28 stalk region [34], [35]. A FLAG-tag was used to enable CAR detection with an anti-FLAG antibody. For the DNA sequences of the respective elements, see Table 3.12 in chapter 3.2.5.

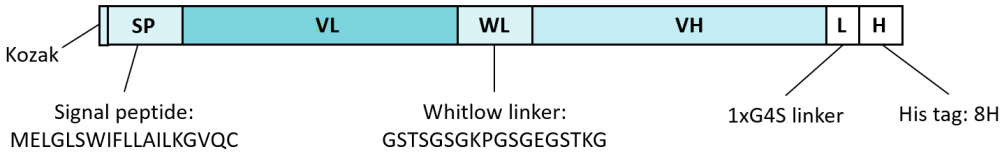

Figure 4.1: ScFv design for soluble expression. For V_L and V_H amino acid sequences, see Table 3.11 in chapter 3.1.9

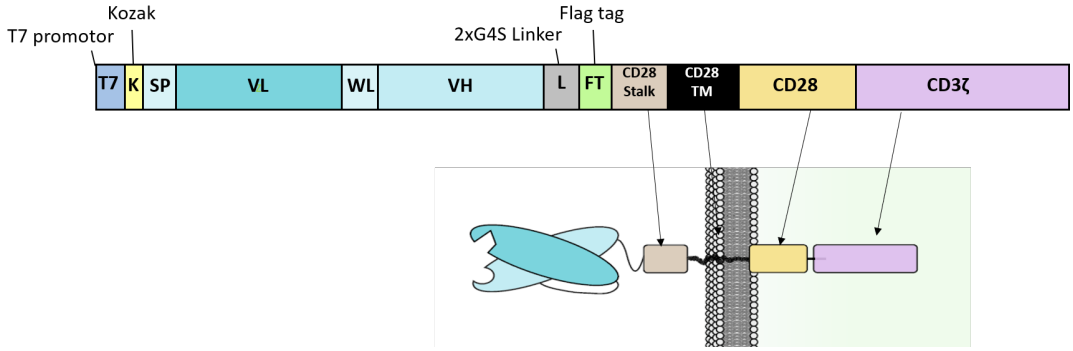

Figure 4.2: CAR construct design for CAR surface expression on Nur77 Jurkat reporter cells. For DNA sequences of CAR backbone elements, see Table 3.12 in chapter 3.1.10 – CAR image by Labanieh et al. [14]

4.3 CAR experiments

4.3.1 CAR construction

For the CAR construction, the genes encoding for the scFv fragments and the CAR backbone were PCR-amplified and subsequently assembled. The assembled CAR constructs were amplified in a second PCR reaction. Figure 4.3 shows examplary agarose gels for 1st (a) and 2nd step (b) PCR products. The left gel shows bands at the expected hight of approximately 900 bp which matches the sequence length of the scFv sequences plus overhangs. Likewise, the gel shows a band at the expected hight of approximately 600 bp for the CAR backbone DNA. The right gel shows bands at the hight of approximately 1500 bp matching the size of correctly assembled CAR DNA. The purified, sequence-verified CAR DNA was then used for *in vitro* transcription into mRNA. Figure 4.4 shows an agarose gel of selected mRNA constructs before and after poly-adenylation. In the lanes of poly(A) mRNA one can see a smear resulting from the poly(A) tail indicating successful poly-adenylation. One can also observe a second faint band in the samples lanes which might be the result of the formation of mRNA secondary structures.

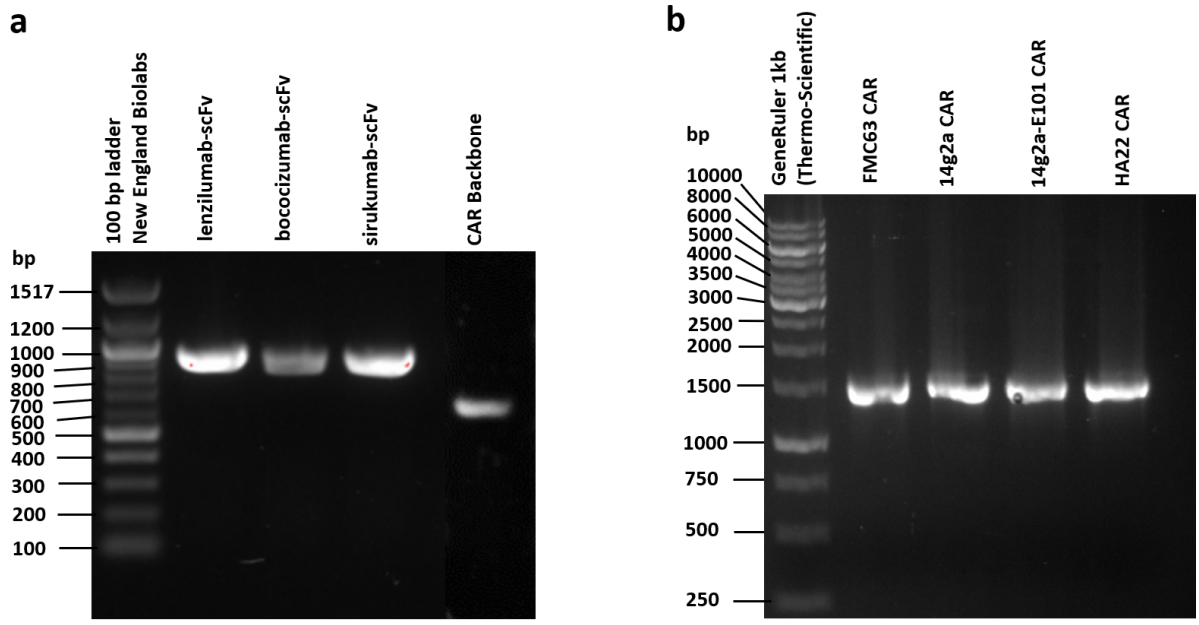

Figure 4.3: Exemplary agarose gels of selected 1st (a) and 2nd step (b) PCR products.

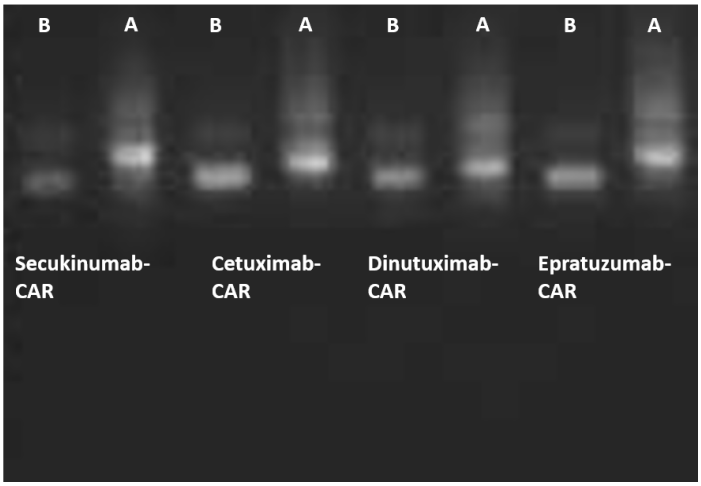

Figure 4.4: Exemplary agarose gel of selected CAR mRNAs before (B) and after (A) poly-adenylation.

4.3.2 Analysis of CARs in Jurkat cells

To analyze the influence of the set of scFvs on the tonic signaling behavior of the respective CARs, the scFvs were expressed on identical CAR backbones as described above and introduced into a Nur77 Jurkat reporter cell line by mRNA electroporation. Exploiting mKusabiraOrange2 (mKO2) as reporter gene, Nur77 overexpression that is specific for antigen receptor signaling could be detected with flow cytometry (Figure 4.5b). As mentioned, the universal CAR design included a FLAG-tag to enable detection of CAR expression levels with flow cytometry using an APC-conjugated anti-FLAG-tag antibody. Experiments were carried out in triplicates. The first two experiments were carried out with the same batch of *in vitro* transcribed mRNA. For the third experiment, a new batch of mRNA was produced. In one of the three experiments, the HA22-based CAR was not expressed which might be attributed to a mistake in the electroporation process. Thus, the presented data for the HA22-based CAR is the result of two measurements only.

CAR expression levels differed greatly among the set of scFvs (Figure 4.5a). The 14g2a-based CAR showed almost no expression. The CAR based on the affinity-matured version of the 14g2a scFv (14g2a-E101K), however, was expressed considerably well. The FMC63-based CAR showed very low expression. Comparing CARs incorporating non-sticky and sticky scFvs, respectively, no trend in terms of expression could be observed. Within both subsets, some CARs were well expressed and other CARs were poorly expressed.

Among the CARs incorporating benchmark scFvs, as expected, basically no tonic signaling could be detected with the FMC63-based CAR. According to current knowledge in the CAR field, we would have expected to see tonic signaling with the 14g2a-based CAR. However, the CAR expression might have been too low to observe a population shift towards tonic signaling. The better expressed 14g2a-E101K-based CAR exhibited clearly detectable tonic signaling. Lastly, the CARs based on the HA22 scFv and the m971 scFv displayed no or only weak tonic signaling.

The CARs based on non-sticky scFvs (marked in mint) mostly displayed very weak tonic signaling. Only the CARs incorporating the dinutuximab scFv and the epratuzumab scFv induced considerable tonic signaling. In contrast, among the CARs based on sticky scFvs (marked in pink), four out of five candidates exhibited noticeably stronger tonic signaling than all tested CARs (lenzilumab scFv, bococizumab scFv, sirukumab scFv and glembatumumab scFv). With the ixekizumab CAR hardly any tonic signaling was observed.

Figure 4.6 shows flow cytometry dot plots of one representative experiment. The plots visualize the correlation between CAR expression and CAR tonic signaling. One can see clearly that tonic signaling is observed for both well (sirukumab scFv, glembatumumab scFv) and poorly (lenzilumab scFv, bococizumab scFv) expressed CARs. The likewise poorly expressed CAR based on the ixekizumab scFv displayed hardly any tonic signaling. In addition, there are CARs which show high expression and no or only weak tonic signaling (HA22 scFv, m971 scFv, trastuzumab scFv, tovetumab scFv, secukinumab scFv, cetuximab scFv). Summing up, various degrees of tonic signaling were detected among the analyzed CARs. With one exception, CARs based on sticky scFvs displayed stronger tonic signaling than CARs based on non-sticky scFvs. The tonic signaling behavior was observed with both highly and poorly expressed CARs.

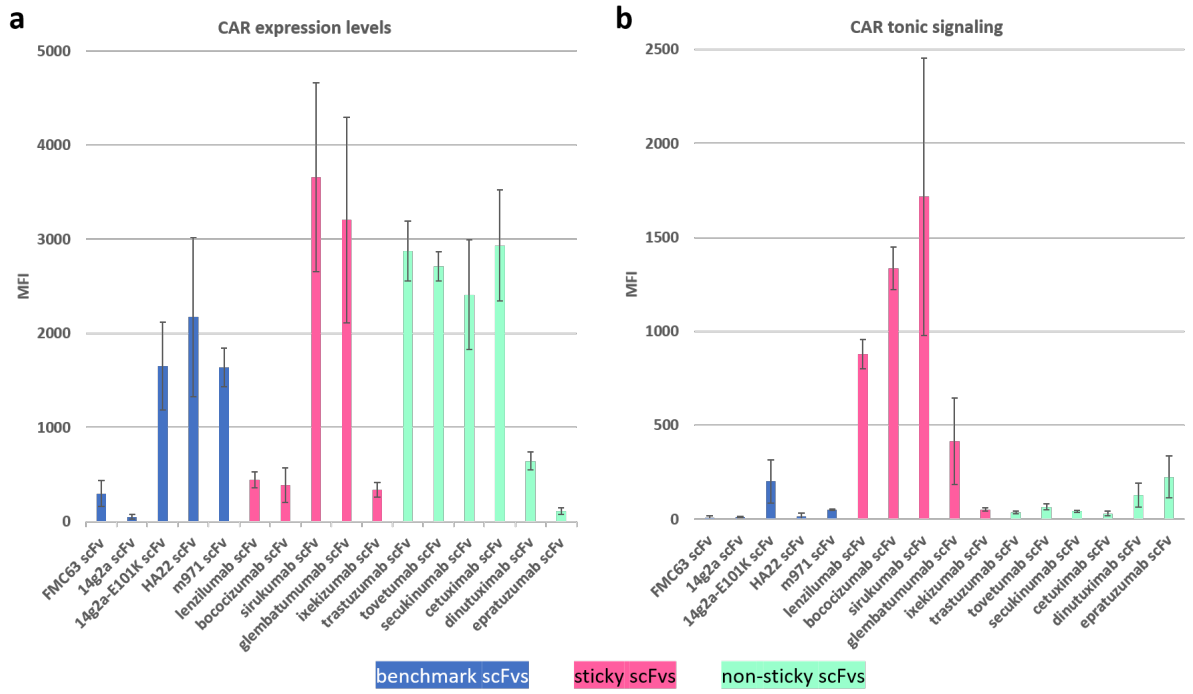

Figure 4.5: (a) CAR expression levels on Jurkat reporter cells approx. 20 hours after mRNA electroporation. Jurkat reporter cells were electroporated with 5 µg mRNA – The geometric means of the fluorescence intensities (MFIs) of the CAR-expressing Jurkat reporter cells were analyzed. The average MFIs ± standard deviations (SDs) of three independent experiments after Mock subtraction are shown (in case of the HA22-based CARs the values are derived from two independent experiments). (b) Tonic signaling activity by reporter gene expression under the Nur77 promotor (MFI). Data are shown as mean ± SD of three independent experiments after Mock subtraction (in case of the HA22-based CARs the values are derived from two independent experiments).

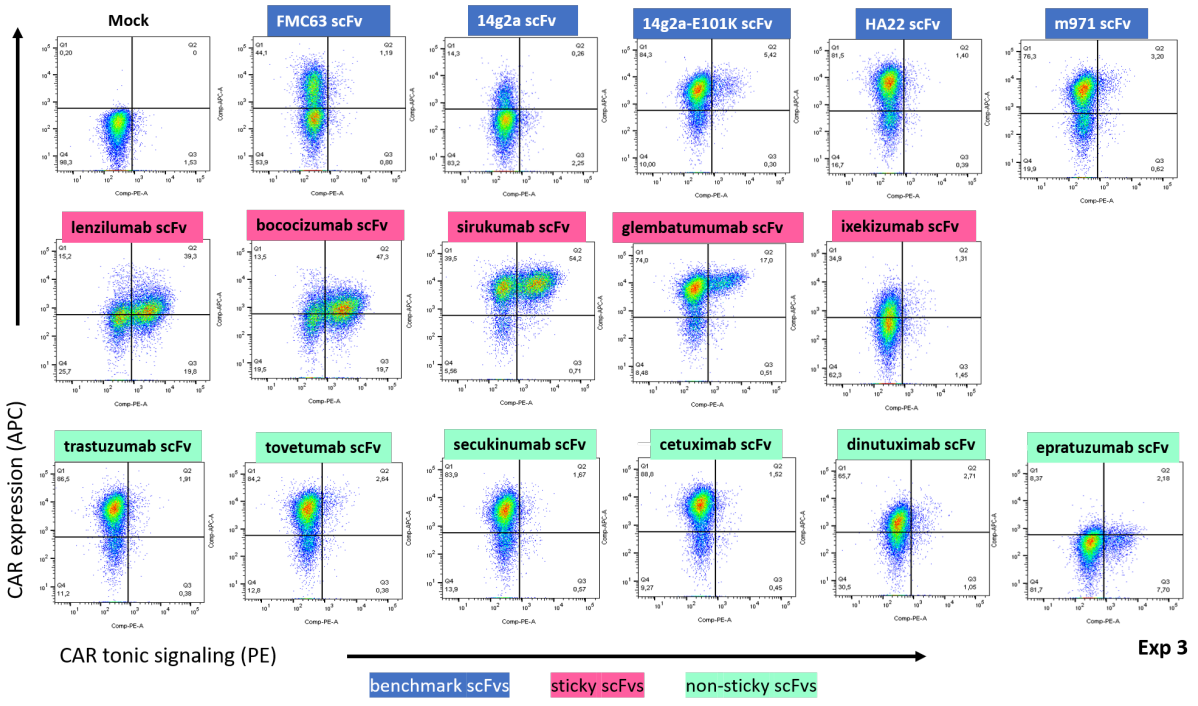

Figure 4.6: Analysis of CAR expression and tonic signaling of all 16 CARs. Shown are flow cytometry dot plots of one representative experiment. For dot plots of remaining experiments, see Supplementary Figure 6.2. Headings for each dot plot refer to the scFv used as CAR-binding domain.

4.3.3 Correlation of the tonic signaling data with the biochemical properties of scFvs according to the Adimab dataset

The tonic signaling data of the analyzed CARs was correlated with the assay results of the respective antibodies derived from the Adimab study (Figure 4.7)[43]. Detailed assay descriptions can be found in the supporting information from the Adimab study [46]. The highest correlation was observed for the affinity-capture self-interaction nanoparticle spectroscopy assays (AC-SINS, SGAC-SINS). In addition, the results of the cross-interaction chromatography (CIC) assay indicate a tendency of longer retention times for scFvs associated with high tonic signaling. Also, bad performances in the poly-specificity assay (PSR), the BVP ELISA assay and the clone self-interaction assay (CSI-BLI) may be correlated with stronger tonic signaling, however, the correlation is less clear. The thermal stability does not show an apparent correlation with the tonic signaling behavior. Similarly, the data from the hydrophobic interaction chromatography (HIC) and the standup monolayer adsorption chromatography (SMAC) assays do not seem to correlate with the tonic signaling behavior.

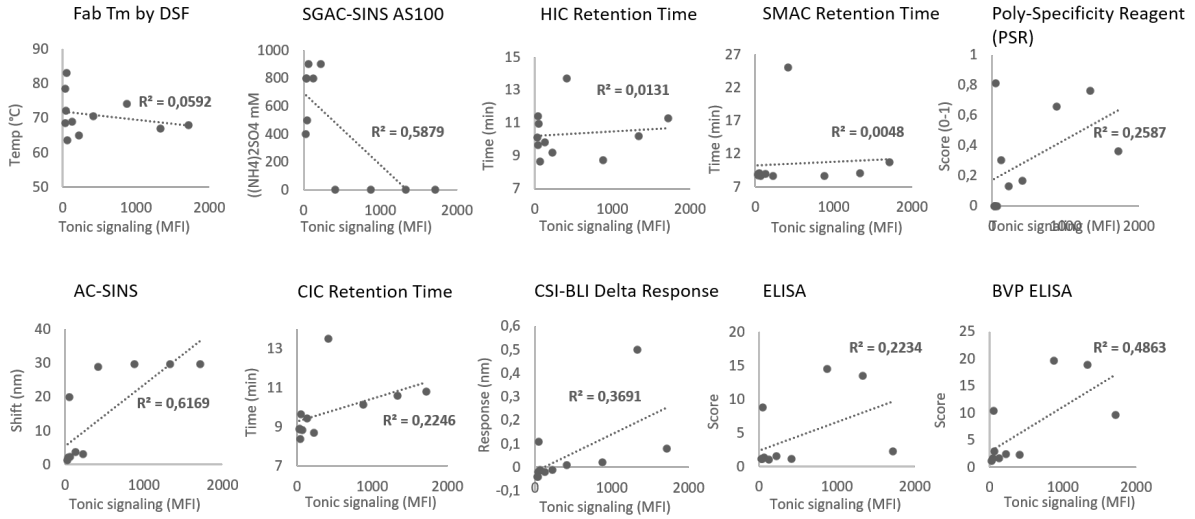

Figure 4.7: Correlation of the tonic signaling data of the analyzed CARs with the assay results of the respective antibodies derived from the Adimab study [43].

4.4 Biochemical characterization of solubly expressed scFvs

We aimed to further investigate the trend we observed in terms of tonic signaling for non-sticky and sticky scFvs by analyzing the scFvs' nonspecific binding and aggregation behavior as well as their thermal stability. Based on our hypothesis that sticky and/or aggregation-prone scFvs lead to more tonic signaling than scFvs with little nonspecific binding and aggregation behavior, we aimed to investigate whether scFvs associated with stronger tonic signaling would exhibit longer retention times in size exclusion chromatography (SEC) measurements. Due to the fact that all scFvs have similar Mws (Table 4.2), noticeably longer retention times can be assumed to be the result of nonspecific binding to the column material. The conjunction with multiangle light scattering (MALS) allows for the determination of the Mws of the measured proteins and thus provides information about the scFvs' aggregation behavior. Moreover, by using MALS detection, it can also be investigated whether delayed peaks represent sticky proteins interacting with the column matrix or degradation products, since the latter would show lower masses. Notably, this assay is similar to the SMAC assay performed in the Adimab study [43]. However, in the SMAC assay a column with a hydrophobic standup monolayer with terminal hydrophilic groups is used [47]. In terms of the scFvs' thermal stability we aimed to perform differential

scanning calorimetry (DSC) measurements to investigate whether thermally less stable scFvs are associated with higher tonic signaling of respective CARs.

ScFv	Theoretical Mw (kDa)
FMC63 scFv	27.9
m971 scFv	28.4
Sirukumab scFv	27.4
Trastuzumab scFv	27.8
Tovetumab scFv	27.7
Secukinumab scFv	29.0
Cetuximab scFv	27.8

Table 4.2: List of theoretical molecular weights of solubly expressed scFvs

4.4.1 Soluble scFv expression

On basis of the tonic signaling data, a selection of scFvs were solubly expressed in HEK293 6E cells and subsequently characterized with SEC-MALS. We aimed to analyze a set of scFvs that were associated with strong tonic signaling as well as a set of scFvs that did not lead to tonic signaling. However, low protein expression in HEK cells as well as protein loss due to precipitation after thawing were limiting in the final scFv selection. As a result, seven scFvs which did not lead to tonic signaling and only one scFv which did lead to tonic signaling (sirukumab scFv) could be analyzed by SEC-MALS (Tables 4.3 and 4.4). Two of the well-expressed scFvs (trastuzumab scFv and secukinumab scFv) were additionally analyzed with DSC.

Table 4.3: HEK titers (in mg/L) of collected scFv expressions. Each row represents the HEK titer achieved in one scFv expression batch.

scFv	HEK titer (mg/L)
FMC63 scFv	1.60
	0.57
	10.00
14g2a scFv	0.10
m971 scFv	5.18
Sirukumab scFv	0.30
Trastuzumab scFv	12.04
Tovetumab scFv	2.91
	1.00
	1.20
	2.00
Secukinumab scFv	13.14
Cetuximab scFv	1.80
	1.00
Dinutuximab scFv	1.60
	0.20
Epratuzumab scFv	0.00

Table 4.4: Final set of scFvs for SEC-MALS measurements

scFv	Tonic signaling
FMC63 scFv	**no/weak**
m971 scFv	
Trastuzumab scFv	
Tovetumab scFv	
Secukinumab scFv	
Cetuximab scFv	
Dinutuximab scFv	
Sirukumab scFv	**strong**

ScFvs were purified with IMAC using HisTALON gravity flow glass columns and TALON resin.

For verification of successful scFv expression and purification, samples from the HEK-supernatant, the TALON flow through, the TALON wash and the purified sample were loaded on SDS PAGE gels. In Figure 4.8 one gel image is shown for illustrative purposes. In the sample lane a single band with the expected Mw of ∼ 28 kDa is visible. At the same height a band is visible in the load lane. The band can neither be observed in the flow through lane nor in the wash lane. Thus, the TALON IMAC process was suitable for scFv purification, since no protein was lost during the purification process and the final protein was very pure.

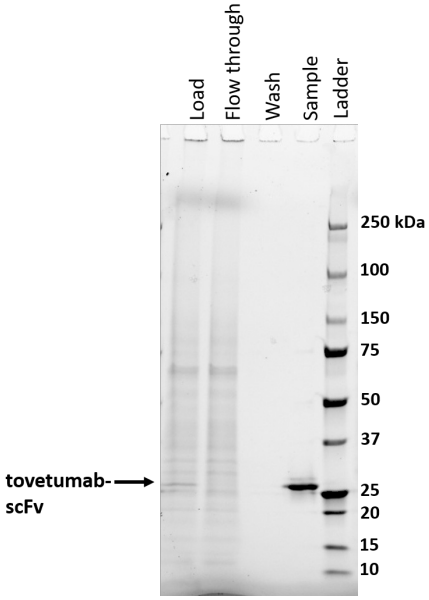

Figure 4.8: Exemplary SDS PAGE gel after scFv purification with TALON resin

4.4.2 Analysis of the thermal stability of scFvs

As mentioned above, the thermal stability of the trastuzumab scFv and the secukinumab scFv were analyzed with DSC. The T_m value represents the temperature at which equal amounts of folded and unfolded protein are present in the sample solution. According to the DSC results (single measurements), the trastuzumab scFv seems to be thermally more stable (T_m=70.7°C) than the secukinumab scFv (T_m=64.6°C)(Figure 4.9). After comparison of the tonic signaling results and the thermal stability of the antibody isotypes within the Adimab dataset, no implications for a correlation between the two could be determined. On this basis and as scFv expression yields were low, DSC measurements were not continued with the rest of the scFv selection.

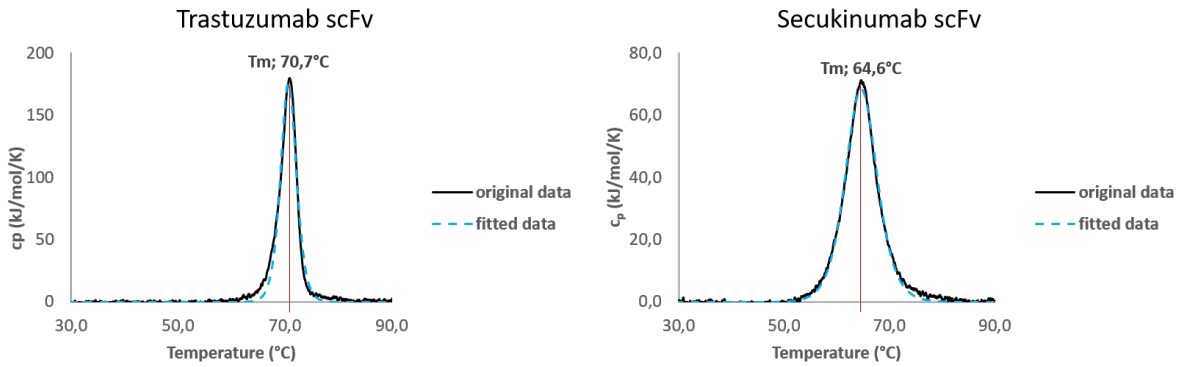

Figure 4.9: DSC curves of trastuzumab scFv and secukinumab scFv (10µM each)

4.4.3 Analysis of the nonspecific binding and aggregation behavior of scFvs

For investigation of the nonspecific binding and aggregation behavior, scFvs were subjected to SEC-MALS measurements. The SEC profiles and the MALS-determined Mws for each peak within the profiles provide information whether scFvs form diabodies or higher aggregates. Figure 4.10 shall give an example of how to interpret a given SEC profile (here the trastuzumab scFv). Peak number one belongs to the fraction that eluted last. According to the MALS measurement a Mw of 32 kDa (+-4%) was determined. The theoretical Mw of this scFv is 27.8 kDa. Thus, one can conclude this peak represents monomeric scFvs. The second peak eluted earlier and a Mw of 65 kDa (+-5%) was determined which is roughly double the Mw of the monomeric scFv fraction indicating that this peak represents dimerized scFvs. Each scFv was analyzed in duplicates. All scFvs were stored at -80°C prior to SEC analysis. From the FMC63 scFv, the tovetumab scFv and the cetuximab scFv two distinct expression batches (DB) were analyzed. The SEC profiles of the duplicate measurements all looked highly similar (Figure 4.11).

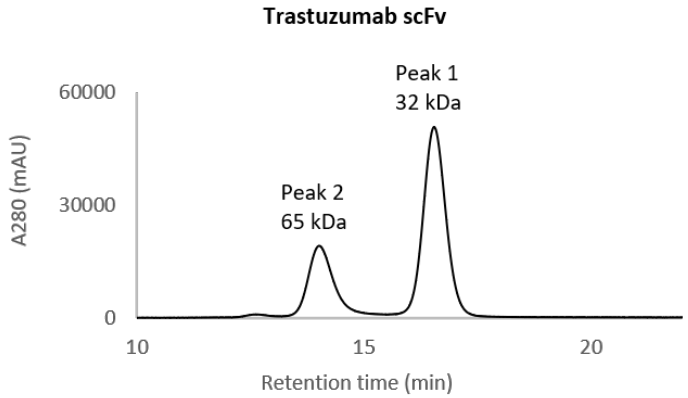

Figure 4.10: Exemplary SEC profile of the trastuzumab scFv showing two peaks with respective Mws as determined by MALS

The comparison of the SEC profiles of the different scFvs shows distinct oligomerization behaviors (Figure 4.11). The SEC profile of the FMC63 scFv exhibits a single monomer peak and a small early-eluting peak which might be the result of higher aggregates. Similarly, the sirukumab scFv, which was associated with high tonic signaling behavior on CARs, eluted in a single monomer peak accompanied by a small elevation at an earlier elution time which might indicate low-level aggregation.

The m971 scFv, the trastuzumab scFv and the cetuximab scFv mainly eluted as monomers, but also formed diabodies to some extent. The SEC profile of the m971 scFv additionally exhibits a small third peak indicating scFv aggregation. The secukinumab scFv eluted primarily as diabodies and also seems to form higher aggregates. Lastly, SEC analysis of the tovetumab scFv implied major aggregation in both of the two distinct expression batches. Summing up, scFvs which were not associated with tonic signaling when expressed on CARs did form diabodies and higher aggregates upon soluble expression. In contrast, the sirukumab scFv did not dimerize and showed little to no aggregation.

The scFvs' MALS-determined Mws were in general higher than the theoretical values (Table 4.6). However, this inaccuracy was also observed for the standard proteins and seems to be a systematic error (Table 4.5). Additionally, low amounts of analyzed proteins increased the inaccuracies. The 1:2 stochiometries between the determined Mws of the first and second peaks strongly suggest the scFvs' monomeric and dimeric states, respectively. Only in case of the tovetumab scFv, the MALS-determined Mws seem to indicate dimers and tetramers. However, the inaccuracy of the measurement was high due to a low sample amount. Moreover, the elution

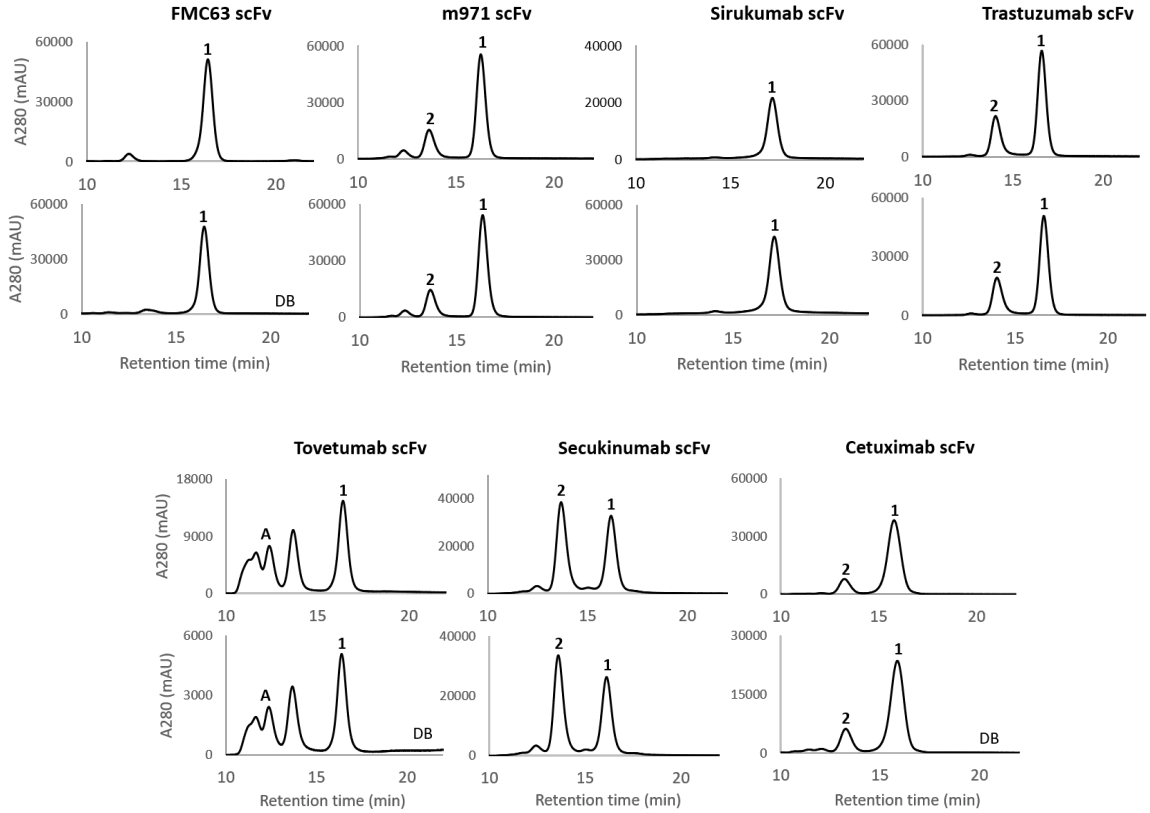

Figure 4.11: Comparison of SEC profiles of scFv duplicate measurements. 1 and 2 indicate monomer and dimer peaks, A indicates aggregates and DB stands for distinct scFv expression batches.

time of the first peak of the tovetumab scFv SEC profile is highly similar to the elution times of the monomer peaks of the other scFvs suggesting that it also represents monomers not dimers (Table 4.7).

Table 4.5: Comparison of theoretical and MALS-determined molecular weights of standard proteins. Results from a single measurement.

Standard	**Theoretical Mw (kDa)**	**MALS-determined Mw (kDa)**
BSA	66.5	72.6 (+-1%)
Ovalbumin	45	46.5 (+-1&)
Myoglobin	16.7	23.7 (+-2%)
Cytochrome c	12	15.4 (+-2%)

Table 4.6: Comparison of theoretical and MALS-determined Mws of scFvs. Results from a single measurement.

ScFv	Theoretical Mw (kDa)	MALS-determined Mw (kDa)	
		Peak 1	Peak 2
FMC63 scFv	27.9	29.9 (+-7%)	
m971 scFv	28.4	32 (+-4%)	68.6 (+-5%)
Sirukumab scFv	27.4	35.5 (+-10%)	
Trastuzumab scFv	27.8	32.2 (+-4%)	64.6 (+-5%)
Tovetumab scFv	27.7	55.5 (+-17%)	126 (+-15%)
Secukinumab scFv	29.0	34.7 (+-5%)	65.6 (+-2%)
Cetuximab scFv	27.8	34.7 (+-4%)	73.1 (+-6%)

Aside from the scFvs's aggregation behavior, the SEC measurements provide information about the scFvs' nonspecific binding behavior. Nonspecific binding to the column material results in a delayed elution time. As already mentioned above, SEC measurements were carried out in duplicates. To be able to estimate the theoretical elution time of the scFvs according to their Mws, four standard proteins covering an appropriate size range were measured within each run. A calibration curve was created using the mean of the standard elution times of both measurements. The mean values of the observed elution times for each scFv were plotted in different colors. The elution times were highly similar for the same scFv between the two measurements with a maximum observed difference of 0.12 minutes and an average difference of 0.04 minutes. Additionally, the theoretical elution times for each scFv were calculated and plotted in the graph (Figure 4.12). All analyzed scFvs eluted later than calculated. The elution time of the cetuximab scFv most closely matched the calculated elution time. The sirukumab scFv exhibited by far the longest elution time of all scFvs analyzed (Table 4.7). This late elution suggests nonspecific binding of the scFv to the SEC-column. Notably, the sirukumab scFv was the only scFv in this set which led to high tonic signaling on CARs.

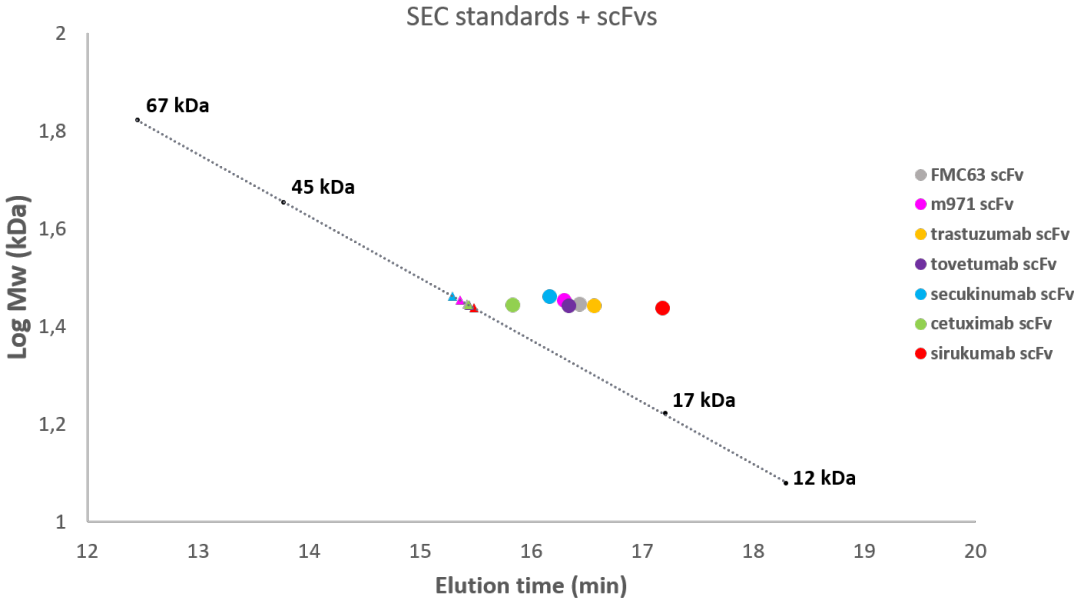

Figure 4.12: SEC standard calibration curve including datapoints of eluted scFvs (circles) and theoretical elution times of analyzed scFvs (triangles). Time points of eluted scFvs are averaged from two independent measurements.

Table 4.7: Comparison of theoretical and observed SEC elution times of analyzed scFvs. The values are averaged from two independent measurements.

scFv	**Theoretical elution time (min)**	**Observed elution time (min)**
FMC63 scFv	15.42	16.43
m971 scFv	15.36	16.30
Sirukumab scFv	15.49	17.18
Trastuzumab scFv	15.44	16.57
Tovetumab scFv	15.45	16.34
Secukinumab scFv	15.29	16.16
Cetuximab scFv	15.43	15.83

Chapter 5

Discussion

Within this work, we analyzed the tonic signaling behavior of a set of 16 CARs which consisted of identical CAR backbones but incorporated different scFvs as binding domains to investigate whether biochemical parameters of scFvs can be correlated with the tonic signaling behavior of respective CARs. The scFv selection consisted of a subset of aggregation-prone and/or sticky scFvs (referred to as sticky scFvs) as well as a subset of non-aggregation-prone and non-sticky scFvs (referred to as non-sticky scFvs). For the selection of sticky and non-sticky scFvs, we exploited an extensive dataset created by the company 'Adimab' which revealed the biophysical properties of a multitude of antibody isotypes [43]. Within both subsets, we included scFvs of different thermal stabilites. In addition, we included a set of scFvs which have been associated with tonic signaling and T cell exhaustion to varying degrees as reported by Long et al. These scFvs should serve as tonic signaling benchmark candidates.

We observed that CARs which incorporated sticky scFvs were tendentially associated with higher tonic signaling than CARs which incorporated non-sticky scFvs. Among the CARs based on non-sticky scFvs, most CARs exhibited only very weak tonic signaling. Two CARs displayed stronger tonic signaling, however to a lesser extent than the majority of CARs based on sticky scFvs. This was in line with our expectations as we hypothesized that CARs based on non-sticky scFvs would neither led to CAR clustering nor interact nonspecifically with cell surface molecules on the same cell or neighboring cells.

In contrast, four out of five CARs based on sticky scFvs displayed noticably stronger tonic signaling than all analyzed CARs. The strongest tonic activation was observed for CARs based on the lenzilumab scFv, the bococizumab scFv and the sirukumab scFv. These scFvs were derived from antibodies which performed particularly poorly in multiple assays of the Adimab study and fell under the 10% of worst performers in all self- and cross-interaction assays as well as in one hydrophobic interaction assay [43]. The CAR based on the glembatumumab scFv also displayed considerable tonic signaling. In the Adimab study the glembatumumab antibody performed poorly in all hydrophobic interaction assays as well as in the cross-interaction chromatography assay and one self-interaction assay. The ixekizumab scFv was the only scFv within the subset of sticky scFvs which hardly induced any tonic signaling when used in a CAR. This was unexpected as the corresponding antibody performed poorly in several self- and cross-interaction assays within the Adimab study implying susceptibility to aggregation and nonspecific binding. At the same time, the antibody was the thermally most stable candidate in our set and performed well in all hydrophobic interaction assays suggesting high overall stability of this protein. However, in general, the antibodies' thermal stability could not be correlated with the tonic signaling behavior of respective CARs (Figure 4.7). Both, CARs which clearly displayed tonic signaling and CARs which displayed no or only weak tonic signaling, incorporated scFvs which were based on antibodies with high and low thermal stability which implies that the scFvs' thermal stability is not of predictive value for the tonic signaling behavior of CARs. As a side note, the thermal

stability of the two scFvs measured within this work (trastuzumab scFv and secukinumab scFv) matched well with the thermal stability of the respective antibodies measured within the Adimab study. The difference in the T_m values was 6.1°C for the scFvs and 6.5°C for the antibodies reported in the Adimab study [43].

These collected observations indicate that scFv self- and/or cross-interactions play an important role in the development of tonic CAR signaling. Nevertheless, considering that the CAR based on the ixekizumab scFv behaved contrary to our expectations, the trend for higher tonic signaling with CARs based on sticky scFvs must be further investigated. For example, this could be done by increasing the sample size of the experiment and by including a scFv similar to the ixekizumab scFv which is susceptible towards self- and cross-interactions but exhibits a noticeably high thermal stability.

Generally, some assays performed within the Adimab study correlated better with the tonic signaling behavior of CARs than others. The data from the affinity-capture self-interaction nanoparticle spectroscopy (AC-SINS) assay as well as from the cross-interaction chromatography (CIC) assay seemed to correlate well with the tonic signaling data (Figure 4.7). In case of the AC-SINS assay the antibody of interest is captured with anti-human Fc polyclonal antibodies immobilized on gold nanoparticles [46]. Upon self-interaction of the captured antibody of interest, the changing atomic distance between the molecules can be detected with a spectrometer due to a change in the absorption wavelength [48]. Bad performance in this assay may not only be the result of self-interaction but could also be the result of non-specific attraction (general stickiness). In case of the other self- and cross-interaction assays (CSI-BLI, PSR, ELISA, BVP ELISA) the correlations were less clear but still apparent. It would be interesting to investigate these correlations for a bigger sample size. In contrast, the results of the hydrophobic interaction assays (HIC and SMAC) did not seem to correlate with tonic signaling.

Interestingly, out of the CARs based on benchmark scFvs only the 14g2a-E101K-based CAR led to considerable tonic T cell activation. Long and colleagues reported different degrees of tonic activation of CARs based on the 14g2a scFv, the HA22 scFv, the m971 scFv and the 4d5 scFv (= trastuzumab scFv) [34]. However, a direct comparison of the group's experiments with our experiments may be difficult as the circumstances of tonic signaling analysis were different. While we analyzed the tonic signaling behavior of transiently expressed CARs *in vitro* in Jurkat reporter cells, Long and colleagues analyzed the tonic activation of CARs in *ex vivo* cultured primary T cells seven days post T cell activation by detecting activation markers. Additionally, discrepancies between our observations and the group's findings may be explained by different scFv and CAR designs. For our analysis, all scFv and CAR constructs had the same design to allow for comparability of tonic signaling results. This was not the case for the scFv and CAR designs applied by Long and colleagues which were different for the CARs based on the HA22 scFv, the m971 scFv and the 4d5 scFv. Although the signaling and transmembrane domains were identical to our constructs as well as among their constructs, the designs differed in the linker length, the V_H-V_L orientation and the occasional inclusion of an IgG1-Fc spacer domain.

Starting the comparison with the FMC63-based CAR, our CAR construct was almost identical to the one used by Long and colleagues and the tonic signaling results matched the findings of the group. As expected, we did not observe tonic activation with this CAR. Concerning the CAR expression, our CAR was poorly expressed while Long et al. did not report poor expression of their FMC63-based CAR. However, they did not only analyze primary T cells instead of Jurkat cells but also used different means of CAR introduction, both of which have an influence on CAR expression levels. Therefore, a comparison of CAR expression levels may not be feasible.

Similarly, CAR expression levels of our 14g2a-based CAR were extremely low which hampered the analysis of the tonic signaling behavior of this CAR. We would have expected high tonic signaling based on the findings from Long and colleagues. However, the group used another linker (details unknown) and included an IgG1-Fc spacer in their 14g2a-based CAR construct

which has previously been shown to promote tonic signaling [49]. Nevertheless, Long et al. did not observe reduced CAR exhaustion upon removal of the spacer domain and introduction of the Whitlow linker as was used in our 14g2a-based CAR, resulting in a CAR design almost identical to ours. Moreover, Long et al. did not observe lower surface expression of this CAR construct compared to their original construct, although the inclusion of an IgG1-Fc spacer domain usually increases CAR expression according to literature [50].

In terms of the HA22-based CAR, Long and colleagues observed only low tonic activation. This roughly matches our findings as the HA22-based CAR displayed hardly any tonic signaling. However, Long et al. included an IgG1-Fc spacer domain in their construct which complicates the comparison of the observations. In addition, the group's construct was built with an opposite V_H-V_L orientation than was used in our scFv constructs. To our knowledge, it has not yet been investigated whether the scFv domain orientation has an influence on the tonic signaling behavior of CARs. Unfortunately, no report on the linker length used in the HA22 scFv could be found. The linker length has a great influence on the scFv aggregation behavior with a shorter linker (<15 amino acids) favoring the formation of oligomers [22]. In all our constructs a Whitlow linker of 18 amino acids in length was used to enable sufficient flexibility and reach for correct V_L-V_H pairing and to ensure proteolytic stability of the linker.

Further, Long et al. observed considerable tonic activation of T cells expressing 4d5-based and m971-based CARs. In our experiments the m971 based CAR induced weak tonic signaling and the 4d5-based CAR induced hardly any tonic signaling. In case of the 4d5-based CAR, this difference may be explained by the use of a shorter linker length by Long and Colleagues. The CAR construct was built with a short version of the Whitlow linker with only 15 amino acids in length which may have been short enough to favor the formation of diabodies. The extent of diabody formation with a certain linker length has been shown to differ among scFvs [51]. According to Long et al.'s findings this could have led to CAR clustering explaining the difference in the observed tonic signaling behavior. Unfortunately, the linker length of the m971 scFv could not be found [34].

Lastly, we also investigated the tonic signaling behavior of a CAR incorporating an affinity-matured version of the 14g2a-based scFv (E101K). The E101K-14g2a-based CAR exhibited a considerably higher surface expression than the 14g2a-based CAR and displayed considerable tonic signaling. We expected to see tonic signaling considering that a E101K-14g2a-based CAR has previously been used as model for tonic signaling to induce T cell exhaustion [40]. However, Lynn and colleagues included an IgG1-Fc spacer domain in their E101K-14g2a-based CAR and no information on the linker length could be found which again complicates a comparison.

In general, no correlation could be observed between the distinct tonic signaling behaviors and the CAR expression levels. High CAR expression levels have been previously shown to favor tonic activation of T cells [52]. However, in our analysis it seems unlikely that the reached CAR expression levels were high enough to have promoted tonic signaling. Some CARs which did no lead to tonic signaling exhibited similarly high expression levels as CARs which were associated with tonic signaling. Moreover, tonic signaling was also observed with poorly expressed CARs indicating that the tonic signaling effects can be primarily attributed to the properties of the scFvs rather than high CAR surface expression.

Interestingly, we found that the tonic signaling behavior of scFv-based CARs does not correlate with the scFvs' tendencies to form dimers or multimers as analyzed by SEC-MALS (Figure 4.11). Dimerization and in part higher aggregation was observed for five out of seven analyzed scFvs highlighting the tendency for diabody formation. In addition, low expression yields within this work may indicate suboptimal stability of the analyzed scFvs. This is in line with previous studies which reported wide variability in scFv stability with low stability often leading to dimer formation, aggregation and low expression yields [22], [53]. Aside from the importance of a long and proteolytically stable linker which has already been discussed above,

the primary scFv sequence plays a key role in scFv stability as shown by Knappik and Plückthun [54]. ScFv molecules do not only lack structural support usually provided by the constant regions in antigen-binding fragments (Fabs) or full-length antibodies but also exhibit solvent-exposed amino acids which are usually part of the interface of the variable and constant regions [36], [55]. This could explain the tendency of some scFvs to form multimers although corresponding antibodies performed well in self-interaction assays. Moreover, the multimerization behavior of solubly expressed scFvs may be distinct from scFvs expressed on CARs. Solubly expressed scFvs encompass certain stresses during production, one example being high intracellular protein concentration prior to secretion which may favor diabody formation [51], [56].

However, the stickiness of scFvs may be a predictive marker for tonic CAR signaling. We observed a noticeably late elution of the sirukumab scFv in the SEC experiments. This scFv induced strong tonic signaling when used in a CAR. Therefore, this SEC result was expected as we hypothesized that scFvs which are associated with high tonic signaling would elute later in the SEC experiments. All other scFvs eluted earlier and were not associated with tonic signaling. Although all scFvs eluted later than calculated according to the calibration curve, the elution time of the sirukumab scFv was 0.8 minute longer than the average elution time of all scFvs analyzed and 0.6 minutes longer than the elution time of the second latest eluting scFv (Figure 4.12). Due to the fact that all analyzed scFvs have a similar size, a longer elution time indicates nonspecific interactions with the column material and thus correlates with the stickiness of the respective scFv. These results imply that tonic signaling may not only be caused by CAR clustering due to scFv self-interaction but also by nonspecific binding of CARs to molecules in the surrounding environment be it to each other or to other molecules expressed on the same cell or neighboring cells. Based on these observations, the investigation of the stickiness of scFvs via SEC measurements may be a suitable approach to predict whether scFvs will perform well or poorly on CARs. However, we are aware that the sample size of the SEC-MALS experiments was clearly too small. Due to low protein expression yields, only one scFv which was associated with tonic signaling was analyzed. Moreover, the likewise SEC-based SMAC assay from the Adimab study did not correlate with the tonic signaling data. Yet, in the SMAC assay a column with a hydrophobic standup monolayer with terminal, hydrophilic groups is used. This assay has been shown to cluster with the HIC assay, where we could not observe a correlation between retention times and tonic signaling either (Figure 4.7) [43]. It is thus essential to further investigate the potential link between scFv stickiness and tonic signaling for example by increasing the sample size before drawing any conclusions.

A logical next step within this project could be the repetition of the experiments with an additional selection of sticky and non-sticky scFvs. Such a scFv validation set would increase the dataset of the tonic signaling experiments and would challenge the observed trend for higher tonic signaling with CARs based on sticky scFvs. Moreover, it could be used to rule out target specific T cell activation in the tonic signaling experiments presented within this work. Although we expect that the observed T cell activation is the result of ligand-independent tonic signaling, our scFv selection comprised scFvs which target antigens secreted by certain T cell lineages. Among them are the ixekizumab scFv and the secukinumab scFv which both target IL-17-A, the lenzilumab scFv which targets the glycoprotein GM-CSF and the sirukumab scFv which targets IL-6. It would be desirable to exclude the possibility that the observed T cell activation is caused by target recognition due to temporary surface association of the secretory antigen to the Jurkat reporter cell surface. The lack of T cell activation with the CARs incorporating the ixekizumab and secukinumab scFvs (targeting IL-17-A) contradicts such a target specific effect. Nevertheless, target specific T cell activation with the CARs based on the lenzilumab and sirukumab scFvs could be ruled out entirely by repeating the tonic signaling experiments with a set of non-sticky scFvs which target the same secretory antigens (GM-CSF and IL-6). A lack of CAR T cell activation would confirm that the secretory antigens are not present and therefore

not recognized on the Jurkat cell surface and that the observed T cell activation was indeed ligand-independent.

The scFv validation set would also increase the sample size of SEC-MALS experiments and could validate the link between scFv stickiness and tonic signaling. However, a broad scFv analysis might not be feasible due to the problem of low scFv expression levels. Alternatively, the validation set could additionally include non-antibody-based scaffolds. Such scaffolds can be engineered to specifically target a certain antigen and have great potential for the use as CAR-binding domains [57]. Ideally, a set of sticky and non-sticky binders should be analyzed to probe whether sticky binders lead to higher tonic signaling than non-sticky binders. Using alternative binding scaffolds in the validation set offers two advantages. First, alternative binding scaffolds are easy to produce in bacterial expression systems. Second, alternative binding scaffolds are monomeric and cannot perform domain swapping. Thus, tonic signaling of CARs incorporating aternative binders cannot be the result of binder dimerization and may be exclusively linked with the binder's stickiness. Taken together, a validation set comprising scFvs and alternative binding scaffolds could increase our understanding of the influence of protein stickiness on the tonic signaling behavior of respective CARs.

In conclusion, we showed that the analysis of the aggregation behavior of solubly expressed scFvs does not constitute a suitable predictive assay for scFv-related tonic signaling of CARs. In contrast, the analysis of the nonspecific binding behavior of scFvs may be of predictive value for tonic signaling as suggested by our results. To our knowledge, no other group has yet linked scFv stickiness with the tonic signaling behavior of CAR T cells. Thus, these findings might change current views and knowledge about the cause of tonic CAR signaling and the selection of scFv candidates used as antigen-binding domains.

Chapter 6

Supplementary material

Antibody	Target	Fab Tm by DSF (°C)	SGAC-SINS AS100 ((NH4)2SO4 mM)	HIC Retention Time (Min)[a]	SMAC Retention Time (Min)[a]	Poly-Specificity Reagent (PSR) SMP Score (0-1)	Affinity-Capture Self-Interaction Nanoparticle Spectroscopy (AC-SINS) Δλmax (nm) Average	CIC Retention Time (Min)	CSI-BLI Delta Response (nm)	ELISA	BVP ELISA
Bad performers											
lenzilumab	GM-CSF	74.0	0.0	8.7	8.6	0.66	29.6	10.1	0.02	14.46	19.60
bococizumab	PCSK9	67.0	0.0	10.2	9.1	0.76	29.6	10.6	0.50	13.50	18.88
sirukumab	IL-6	68.0	0.0	11.3	10.8	0.36	29.6	10.8	0.08	2.17	9.66
glembatumumab	NMB	70.5	0.0	13.7	***25.0***	0.17	***28.9***	***13.5***	0.01	1.06	2.22
ixekizumab	IL-17A	83.0	500.0	10.9	9.1	0.81	20.0	9.6	0.11	8.80	10.40
Good performers											
trastuzumab	Her2	78.5	800.0	9.7	8.8	0.00	2.0	8.8	-0.02	1.06	1.34
tovetumab	RTK: PDGFRA	63.5	900.0	8.7	8.6	0.00	2.2	8.8	-0.01	1.35	2.95
secukinumab	IL-17A	72.0	800.0	11.4	8.9	0.00	-0.6	8.4	-0.04	1.09	1.69
cetuximab	EGFR	68.5	400.0	10.1	8.9	0.00	1.3	8.9	-0.04	1.09	1.09
dinutuximab	GD2	69.0	800.0	9.8	9.0	0.30	3.6	9.4	-0.02	1.03	1.69
epratuzumab	CD22	65.0	900.0	9.2	8.6	0.13	3.0	8.7	-0.01	1.47	2.34
Min		59.5	0.0	8.5	8.5	0.00	-1.1	8.3	-0.05	0.89	1.03
Max		91.5	1000.0	25.0	25.0	0.81	29.9	13.5	0.60	14.46	22.75
Worst 10% threshold			370.0	11.7	12.8	0.27	11.8	10.1	0.01	1.90	4.30

Figure 6.1: Results of the biophysical assays from the Adimab study [43]. Min and Max are the minimum and maximum values achieved among the 137 analyzed antibody isotypes. When an assay result of an antibody was worse than the 10% threshold value marking the worst performing antibodies of all analyzed candidates, the result was marked in red indicating bad performance in that assay. Green fields indicate good assay performance. The assays assessed hydrophobic interactions (SGAC100, SMAC, HIC) self-interactions (CSI, AC-SINS), cross-interactions (CIC, PSR, ELISA assays) and thermal stabilities. A detailed description of the assays can be found in the publication by Jain and colleagues [46]

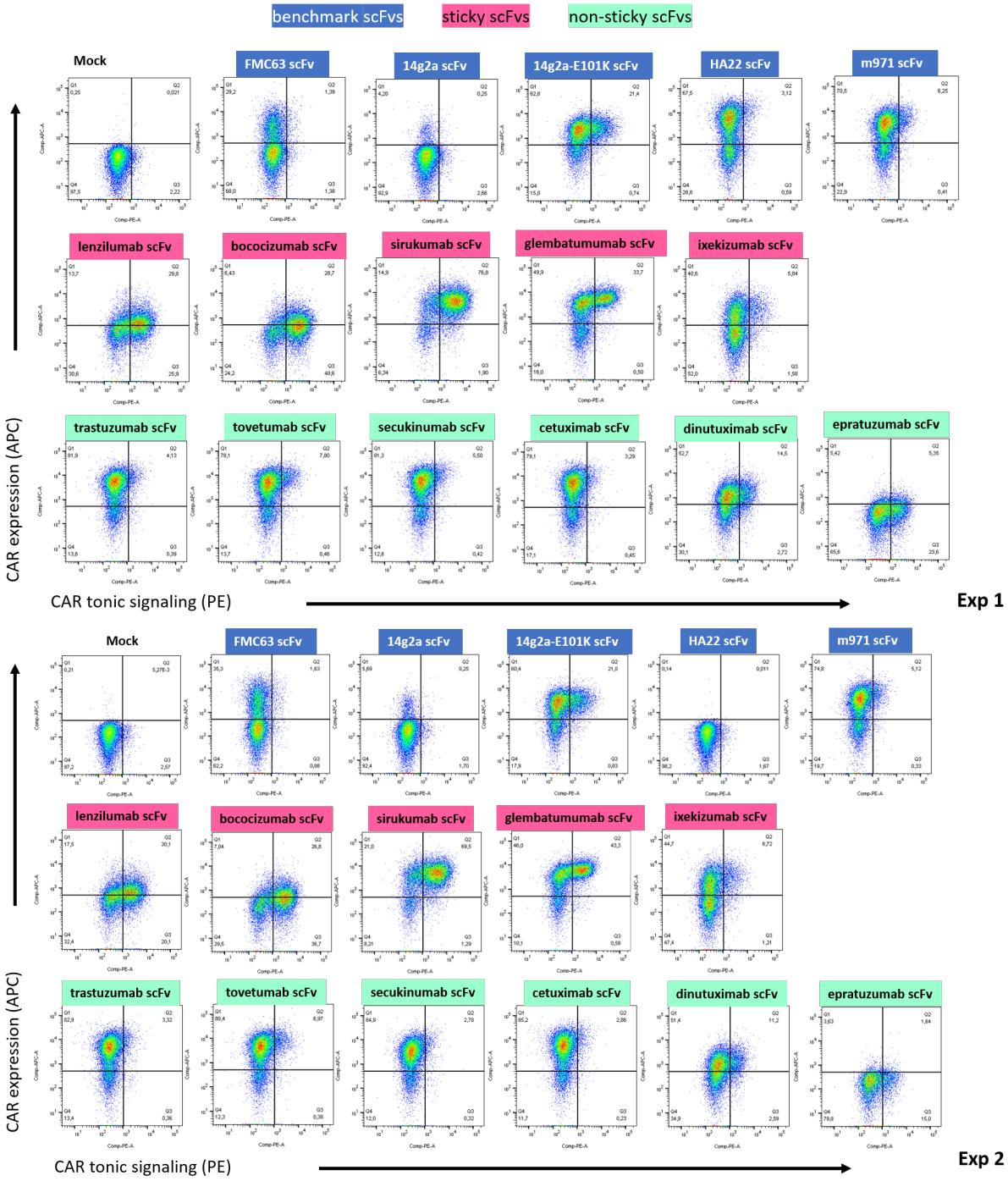

Figure 6.2: Flow cytometry dot plots of experiments one and two. Dot plots of the third experiment are shown in the results section. Headings for each dot plot refer to the scFv used as CAR binding domain.

Bibliography

[1] K. Töpfer, S. Kempe, N. Müller, M. Schmitz, M. Bachmann, M. Cartellieri, G. Schackert, and A. Temme, "Tumor evasion from T cell surveillance," *Journal of Biomedicine and Biotechnology*, vol. 2011, 2011.

[2] A. M. Cornel, I. L. Mimpen, and S. Nierkens, "MHC class I downregulation in cancer: Underlying mechanisms and potential targets for cancer immunotherapy," *Cancers*, vol. 12, no. 7, pp. 1–33, 2020.

[3] F. Garrido, N. Aptsiauri, E. M. Doorduijn, A. M. Garcia Lora, and T. van Hall, "The urgent need to recover MHC class I in cancers for effective immunotherapy," *Current Opinion in Immunology*, vol. 39, pp. 44–51, 2016.

[4] Z. Eshhar, T. Waks, G. Gross, and D. G. Schindler, "Specific activation and targeting of cytotoxic lymphocytes through chimeric single chains consisting of antibody-binding domains and the γ or ζ subunits of the immunoglobulin and T-cell receptors," *Proceedings of the National Academy of Sciences of the United States of America*, vol. 90, no. 2, pp. 720–724, 1993.

[5] S. J. Schuster, J. Svoboda, S. Dwivedy Nasta, D. L. Porter, E. A. Chong, D. J. Landsburg, A. R. Mato, S. F. Lacey, J. J. Melenhorst, A. Chew, J. Hasskarl, G. D. Shah, M. A. Wasik, K. T. Marcucci, Z. Zheng, B. L. Levine, and C. H. June, "Sustained Remissions Following Chimeric Antigen Receptor Modified T Cells Directed Against CD19 (CTL019) in Patients with Relapsed or Refractory CD19+ Lymphomas," *Blood*, vol. 126, no. 23, pp. 183–183, 2015.

[6] R. J. Brentjens, M. L. Davila, I. Riviere, J. Park, X. Wang, L. G. Cowell, S. Bartido, J. Stefanski, C. Taylor, M. Olszewska, O. Borquez-Ojeda, J. Qu, T. Wasielewska, Q. He, Y. Bernal, I. V. Rijo, C. Hedvat, R. Kobos, K. Curran, P. Steinherz, J. Jurcic, T. Rosenblat, P. Maslak, M. Frattini, and M. Sadelain, "CD19-targeted T cells rapidly induce molecular remissions in adults with chemotherapy-refractory acute lymphoblastic leukemia," *Science Translational Medicine*, vol. 5, no. 177, 2013.

[7] S. L. Maude, N. Frey, P. A. Shaw, R. Aplenc, D. M. Barrett, N. J. Bunin, A. Chew, V. E. Gonzalez, Z. Zheng, S. F. Lacey, Y. D. Mahnke, J. J. Melenhorst, S. R. Rheingold, A. Shen, D. T. Teachey, B. L. Levine, C. H. June, D. L. Porter, and S. A. Grupp, "Chimeric antigen receptor T cells for sustained remissions in leukemia," *New England Journal of Medicine*, vol. 371, no. 16, pp. 1507–1517, 2014.

[8] C. H. June and M. Sadelain, *Chimeric antigen receptor therapy*, 2018.

[9] L. Schultz and C. Mackall, "Driving CAR T cell translation forward," *Science Translational Medicine*, vol. 11, no. 481, pp. 1–4, 2019.

[10] Amy Yip and Rachel M. Webster, *The market for chimeric antigen receptor T cell therapies*, 2018.

[11] S. Guedan, H. Calderon, A. D. Posey, and M. V. Maus, "Engineering and Design of Chimeric Antigen Receptors," *Molecular Therapy - Methods and Clinical Development*, vol. 12, no. March, pp. 145–156, 2019.

[12] R. G. Majzner and C. L. Mackall, *Clinical lessons learned from the first leg of the CAR T cell journey*, 2019.

[13] J. Buechner, M. J. Kersten, M. Fuchs, F. Salmon, and U. Jäger, "Chimeric Antigen Receptor-T Cell Therapy: Practical Considerations for Implementation in Europe," *HemaSphere*, vol. 2, no. 1, pp. 1–11, 2018.

[14] L. Labanieh, R. G. Majzner, and C. L. Mackall, *Programming CAR-T cells to kill cancer*, 2018.

[15] B. Savoldo, C. A. Ramos, E. Liu, M. P. Mims, M. J. Keating, G. Carrum, R. T. Kamble, C. M. Bollard, A. P. Gee, Z. Mei, H. Liu, B. Grilley, C. M. Rooney, H. E. Heslop, M. K. Brenner, and G. Dotti, "CD28 costimulation improves expansion and persistence of chimeric antigen receptor–modified T cells in lymphoma patients," *The journal of clinical investigation*, vol. 121, no. 5, pp. 1–5, 2011.

[16] E. Drent, R. Poels, R. Ruiter, N. W. Van De Donk, S. Zweegman, H. Yuan, J. De Bruijn, M. Sadelain, H. M. Lokhorst, R. W. Groen, T. Mutis, and M. Themeli, "Combined CD28 and 4-1BB costimulation potentiates affinity-tuned chimeric antigen receptor-engineered t cells," *Clinical Cancer Research*, vol. 25, no. 13, pp. 4014–4025, 2019.

[17] N. E. Weisser and J. C. Hall, "Applications of single-chain variable fragment antibodies in therapeutics and diagnostics," *Biotechnology Advances*, vol. 27, no. 4, pp. 502–520, 2009.

[18] P. S. Chowdhury and G. Vasmatzis, "Engineering scFvs for improved stability.," *Methods in molecular biology (Clifton, N.J.)*, vol. 207, pp. 237–254, 2003.

[19] K. Zhang, M. L. Geddie, N. Kohli, T. Kornaga, D. B. Kirpotin, Y. Jiao, R. Rennard, D. C. Drummond, U. B. Nielsen, L. Xu, and A. A. Lugovskoy, "Comprehensive optimization of a single-chain variable domain antibody fragment as a targeting ligand for a cytotoxic nanoparticle," *mAbs*, vol. 7, no. 1, pp. 42–52, 2015.

[20] K. Fujiwara, M. Masutani, M. Tachibana, and N. Okada, "Impact of scFv structure in chimeric antigen receptor on receptor expression ef fi ciency and antigen recognition properties," *Biochemical and Biophysical Research Communications*, no. xxxx, 2020.

[21] M. Whitlow, D. Filpula, M. L. Rollence, S. L. Feng, and J. F. Wood, "Multivalent fvs: Characterization of single-chain Fv oligomers and preparation of a bispecific Fv," *Protein Engineering, Design and Selection*, vol. 7, no. 8, pp. 1017–1026, 1994.

[22] A. Wörn and A. Plückthun, *Stability engineering of antibody single-chain Fv fragments*, 2001.

[23] Z. Shen, H. Yan, Y. Zhang, R. L. Mernaugh, and X. Zeng, "Engineering peptide linkers for scFv immunosensors," *Analytical Chemistry*, vol. 80, no. 6, pp. 1910–1917, 2008.

[24] M. Whitlow, B. A. Bell, S. L. Feng, D. Filpula, K. D. Hardman, S. L. Hubert, M. L. Rollence, J. F. Wood, M. E. Schott, D. E. Milenic, T. Yokota, and J. Schlom, "An improved linker for single-chain fv with reduced aggregation and enhanced proteolytic stability," Tech. Rep. 8, 1993, pp. 989–995.

[25] C. L. Bonifant, H. J. Jackson, R. J. Brentjens, and K. J. Curran, "Toxicity and management in CAR T-cell therapy," *Molecular Therapy - Oncolytics*, vol. 3, no. January, p. 16 011, 2016.

[26] S. S. Neelapu, S. Tummala, P. Kebriaei, W. Wierda, C. Gutierrez, F. L. Locke, K. V. Komanduri, Y. Lin, N. Jain, N. Daver, J. Westin, A. M. Gulbis, M. E. Loghin, J. F. De Groot, S. Adkins, S. E. Davis, K. Rezvani, P. Hwu, and E. J. Shpall, "Chimeric antigen receptor T-cell therapy-assessment and management of toxicities," *Nature Reviews Clinical Oncology*, vol. 15, no. 1, pp. 47–62, 2018.

[27] C. Graham, R. Hewitson, A. Pagliuca, and R. Benjamin, "cancer immunotherapy with CAR-T cells - behold the future," *ORIGINAL RESEARCH CME HAEMATOLOGY Clinical*, vol. 18, no. 4, pp. 324–8, 2018.

[28] J. Gust, K. A. Hay, L. A. Hanafi, D. Li, D. Myerson, L. F. Gonzalez-Cuyar, C. Yeung, W. C. Liles, M. Wurfel, J. A. Lopez, J. Chen, D. Chung, S. H. Baker, T. Ozpolat, K. R. Fink, S. R. Riddell, D. G. Maloney, and C. J. Turtle, "Endothelial activation and blood–brain barrier disruption in neurotoxicity after adoptive immunotherapy with CD19 CAR-T cells," *Cancer Discovery*, vol. 7, no. 12, pp. 1404–1419, 2017.

[29] B. Hou, Y. Tang, W. Li, Q. Zeng, and D. Chang, "Efficiency of CAR-T Therapy for Treatment of Solid Tumor in Clinical Trials: A Meta-Analysis," *Disease Markers*, vol. 2019, 2019.

[30] W. A. Lim1 and C. H. June, "The Principles of Engineering Immune Cells to Treat Cancer," *Cell*, vol. 168, no. 4, pp. 724–740, 2017.

[31] S. Srivastava and S. R. Riddell, "Chimeric Antigen Receptor T Cell Therapy: Challenges to Bench-to-Bedside Efficacy," *The Journal of Immunology*, vol. 200, no. 2, pp. 459–468, 2018.

[32] N. Tokarew, J. Ogonek, S. Endres, M. von Bergwelt-Baildon, and S. Kobold, "Teaching an old dog new tricks: next-generation CAR T cells," *British Journal of Cancer*, vol. 120, no. 1, pp. 26–37, 2019.

[33] Bird; Bordon; Minton, "Overcoming CAR T cell exhaustion/ Myeloid PD1 in the frame / Bad mutants in IBD," *Nature*, vol. 20, no. February, pp. 72–73, 2020.

[34] A. H. Long, W. M. Haso, J. F. Shern, K. M. Wanhainen, M. Murgai, M. Ingaramo, J. P. Smith, A. J. Walker, M. E. Kohler, V. R. Venkateshwara, R. N. Kaplan, G. H. Patterson, T. J. Fry, R. J. Orentas, and C. L. Mackall, "4-1BB costimulation ameliorates T cell exhaustion induced by tonic signaling of chimeric antigen receptors," *Nature Medicine*, vol. 21, no. 6, pp. 581–590, 2015.

[35] A. I. Salter, R. G. Ivey, J. J. Kennedy, V. Voillet, A. Rajan, E. J. Alderman, U. J. Voytovich, C. Lin, D. Sommermeyer, L. Liu, J. R. Whiteaker, R. Gottardo, A. G. Paulovich, and S. R. Riddell, "Phosphoproteomic analysis of chimeric antigen receptor signaling reveals kinetic and quantitative differences that affect cell function," *Science Signaling*, vol. 11, no. 544, pp. 1–18, 2018.

[36] A. Ajina and J. Maher, "Strategies to address chimeric antigen receptor tonic signaling," *Molecular Cancer Therapeutics*, vol. 17, no. 9, pp. 1795–1815, 2018.

[37] O. U. Kawalekar, R. S. O'Connor, J. A. Fraietta, L. Guo, S. E. McGettigan, A. D. Posey, P. R. Patel, S. Guedan, J. Scholler, B. Keith, N. Snyder, I. Blair, M. C. Milone, and C. H. June, "Distinct Signaling of Coreceptors Regulates Specific Metabolism Pathways and Impacts Memory Development in CAR T Cells," *Immunity*, vol. 44, no. 2, pp. 380–390, 2016.

[38] S. J. C. Van Der Stegen, M. Hamieh, and M. Sadelain, "The pharmacology of second-generation chimeric antigen receptors," *Nature Reviews Drug Discovery*, vol. 14, no. 7, pp. 499–509, 2015.

[39] Z. Zhao, M. Condomines, S. J. van der Stegen, F. Perna, C. C. Kloss, G. Gunset, J. Plotkin, and M. Sadelain, "Structural Design of Engineered Costimulation Determines Tumor Rejection Kinetics and Persistence of CAR T Cells," *Cancer Cell*, vol. 28, no. 4, pp. 415–428, 2015.

[40] R. C. Lynn, E. W. Weber, E. Sotillo, D. Gennert, P. Xu, Z. Good, H. Anbunathan, J. Lattin, R. Jones, V. Tieu, S. Nagaraja, J. Granja, C. F. de Bourcy, R. Majzner, A. T. Satpathy, S. R. Quake, M. Monje, H. Y. Chang, and C. L. Mackall, "c-Jun overexpression in CAR T cells induces exhaustion resistance," *Nature*, vol. 576, no. 7786, pp. 293–300, 2019.

[41] T. Hart, M. Chandrashekhar, M. Aregger, Z. Steinhart, K. R. Brown, G. MacLeod, M. Mis, M. Zimmermann, A. Fradet-Turcotte, S. Sun, P. Mero, P. Dirks, S. Sidhu, F. P. Roth, O. S. Rissland, D. Durocher, S. Angers, and J. Moffat, "High-Resolution CRISPR Screens Reveal Fitness Genes and Genotype-Specific Cancer Liabilities," *Cell*, vol. 163, no. 6, pp. 1515–1526, 2015.

[42] J. F. Ashouri and A. Weiss, "Endogenous Nur77 Is a Specific Indicator of Antigen Receptor Signaling in Human T and B Cells," *The Journal of Immunology*, vol. 198, no. 2, pp. 657–668, 2017.

[43] T. Jain, T. Sun, S. Durand, A. Hall, N. R. Houston, J. H. Nett, B. Sharkey, B. Bobrowicz, I. Caffry, Y. Yu, Y. Cao, H. Lynaugh, M. Brown, H. Baruah, L. T. Gray, E. M. Krauland, Y. Xu, M. Vásquez, and K. D. Wittrup, "Biophysical properties of the clinical-stage antibody landscape," *Proceedings of the National Academy of Sciences of the United States of America*, vol. 114, no. 5, pp. 944–949, 2017.

[44] I. Horwacik, P. Golik, P. Grudnik, M. Kolinski, M. Zdzalik, H. Rokita, and G. Dubin, "Structural basis of GD2 ganglioside and mimetic peptide recognition by 14G2a antibody," *Molecular and Cellular Proteomics*, vol. 14, no. 10, pp. 2577–2590, 2015.

[45] R. Haryadi, S. Ho, Y. J. Kok, H. X. Pu, L. Zheng, N. A. Pereira, B. Li, X. Bi, L. T. Goh, Y. Yang, and Z. Song, "Optimization of heavy chain and light chain signal peptides for high level expression of therapeutic antibodies in CHO cells," *PLoS ONE*, vol. 10, no. 2, pp. 1–16, 2015.

[46] T. Jain, T. Sun, S. Durand, A. Hall, N. R. Houston, J. H. Nett, B. Sharkey, B. Bobrowicz, I. Caffry, Y. Yu, Y. Cao, H. Lynaugh, M. Brown, H. Baruah, L. T. Gray, E. M. Krauland, Y. Xu, M. Vásquez, and K. D. Wittrup, "Supporting Information - Biophysical properties of the clinical-stage antibody landscape," *Proceedings of the National Academy of Sciences of the United States of America*, vol. 114, no. 5, pp. 944–949, 2017.

[47] N. Kohli and M. L. Geddie, "Novel HPLC-based screening method to assess developability of antibody-like molecules," *Methods in Molecular Biology*, vol. 1575, no. 4, pp. 189–196, 2017.

[48] Y. Liu, I. Caffry, J. Wu, S. B. Geng, T. Jain, T. Sun, F. Reid, Y. Cao, P. Estep, Y. Yu, M. Vaśquez, P. M. Tessier, and Y. Xu, "High-throughput screening for developability during early-stage antibody discovery using self-interaction nanoparticle spectroscopy," *mAbs*, vol. 6, no. 2, pp. 483–492, 2014.

[49] N. Watanabe, P. Bajgain, S. Sukumaran, S. Ansari, H. E. Heslop, C. M. Rooney, M. K. Brenner, A. M. Leen, and J. F. Vera, "Fine-tuning the CAR spacer improves T-cell potency," *OncoImmunology*, vol. 5, no. 12, pp. 1–14, 2016.

[50] A. Hombach, A. A. Hombach, and H. Abken, "Adoptive immunotherapy with genetically engineered T cells: Modification of the IgG1 Fc spacer domain in the extracellular moiety of chimeric antigen receptors avoids off-target activation and unintended initiation of an innate immune response," *Gene Therapy*, vol. 17, no. 10, pp. 1206–1213, 2010.

[51] K. M. Arndt, K. M. Müller, and A. Plückthun, "Factors Influencing the Dimer to Monomer Transition of an Antibody Single-Chain Fv Fragment †," Tech. Rep., 1998.

[52] M. J. Frigault, J. Lee, M. C. Basil, C. Carpenito, S. Motohashi, J. Scholler, O. U. Kawalekar, S. Guedan, S. E. McGettigan, A. D. Posey, S. Ang, L. J. Cooper, J. M. Platt, F. B. Johnson, C. M. Paulos, Y. Zhao, M. Kalos, M. C. Milone, and C. H. June, "Identification of chimeric antigen receptors that mediate constitutive or inducible proliferation of T cells," *Cancer Immunology Research*, vol. 3, no. 4, pp. 356–367, 2015.

[53] S. Ewert, T. Huber, A. Honegger, and A. Plückthun, "Biophysical properties of human antibody variable domains," *Journal of Molecular Biology*, vol. 325, no. 3, pp. 531–553, 2003.

[54] A. Knappik and A. Plückthun, "Engineered turns of a recombinant antibody improve its in vivo folding," *Protein Engineering, Design and Selection*, vol. 8, no. 1, pp. 81–89, 1995.

[55] L. Nieba, A. Honegger, C. Krebber, and A. Plückthun, "Disrupting the hydrophobic patches at the antibody variable/constant domain interface: Improved in vivo folding and physical characterization of an engineered scFv fragment," *Protein Engineering*, vol. 10, no. 4, pp. 435–444, 1997.

[56] A. Oprins, C. Rabouille, G. Posthuma, J. Klumperman, H. J. Geuze, and J. W. Slot, "The ER to Golgi interface is the major concentration site of secretory proteins in the exocrine pancreatic cell," *Traffic*, vol. 2, no. 11, pp. 831–838, 2001.

[57] C. U. Zajc, B. Salzer, J. M. Taft, S. T. Reddy, M. Lehner, and M. W. Traxlmayr, "Driving CARs with alternative navigation tools – the potential of engineered binding scaffolds," *FEBS Journal*, pp. 1–16, 2020.